# *Estimating the filtering of turbulence properties by finite-sized particles using analytical energy spectra*

Article

Accepted Version

# Estimating the filtering of turbulence properties by finite-sized particles using analytical energy spectra

Miguel A. C. Teixeira[1, a)] and Catherine A. Mériaux[2, 3, 4]
[1)] *Department of Meteorology, University of Reading, Reading RG6 6ET, UK*
[2)] *School of Earth, Atmosphere and Environment, Monash University, Clayton, Victoria 3800, Australia*
[3)] *ICTP-East African Institute for Fundamental Science, University of Rwanda, Kigali, Rwanda*
[4)] *International Centre for Theoretical Physics (ICTP), I-34151 Trieste, Italy*

(Dated: 26 March 2022)

Finite-sized neutrally-buoyant particles suspended in a turbulent flow do not typically follow the fluid motion, whereas sufficiently small neutrally-buoyant particles, known as tracers, do. Turbulence properties probed by the two types of particles thus differ primarily due to spatial filtering, whereby scales of motion in the energy spectrum smaller than the particle diameter $D$ are suppressed, whereas those larger are retained. In this study, this filtering effect is quantified for flows with Reynolds numbers in the range $Re_\lambda \approx 32 - 2000$ using a model of isotropic and homogeneous turbulence based on analytical wavenumber and Lagrangian frequency energy spectra. The coefficients scaling these spectra are estimated by comparing the dissipation rate, amplitude of the frequency spectrum and acceleration variance for the fluid motion, as well as the acceleration and velocity variances of the particle motion, with laboratory experiments and numerical simulations. The model reproduces scalings for the acceleration variances of both the fluid and the particles at high Reynolds number. The model is then used to predict the ratios of the velocity variance, acceleration variance, and dissipation rate obtained from the particles to those of the flow. These ratios depart from 1 as $D$ increases (as expected), but the fluid velocity variance is much less severely underestimated by the particle motion than the acceleration variance and dissipation rate, for given $D$ and $Re_\lambda$. These results allow delimiting more systematically the conditions under which finite-sized neutrally-buoyant particles could be as useful to probe turbulent flows as tracer particles in laboratory experiments.

## I. INTRODUCTION

The behaviour of finite-sized neutrally-buoyant particles suspended in a turbulent flow, more specifically their dispersion or clustering, has been investigated in a number of studies[1–5]. Some characteristics of the turbulent flow itself may be inferred from such particles, provided their seeding concentration in the fluid is very low. Even so, using any neutrally-buoyant particles to directly probe the turbulence is regarded as unreliable, unless they exactly follow the fluid motion, which typically only occurs when they approach a microscopic size. Such particles are known as tracers. In practice, a particle is considered to behave as a tracer when the ratio of its diameter $D$ to the Kolmogorov microscale $\eta$ is $D/\eta \lesssim 5$ (Ref. 6) or $D/\eta \lesssim 10$ (Ref. 7), and when in that range, it can be used to infer the turbulence properties of the fluid with all its scales.

In contrast to this standard approach, Mériaux *et al.*[8] recently used finite-sized ($D/\eta = O(100)$) particles to estimate the characteristic scales of an experimental turbulent flow. Lagrangian particle velocity statistics were used to estimate the energy dissipation rate, and the accuracy of this calculation was asserted using qualitative arguments based on the distribution of energy among the turbulence spectrum. Although primary scales derived from these estimates were *a posteriori* shown to provide consistent dispersion regimes within their temporal and spatial limits, the extent to which finite-sized particles could be used to infer statistical properties of turbulent flow was not systematically assessed. A first step in that direction will be taken in the present study.

Unlike so-called 'inertial particles', which have a density different from that of the fluid[9–11], neutrally-buoyant particles are not subject to inertial effects. They may still move relative to the fluid, generating small-scale turbulence in their wake[3,12] if their Reynolds number is large enough, hence modifying the ambient flow. However, the leading-order effect of the particles is simply filtering the fluid motion at spatial scales smaller than their own, as they only follow the motion of larger turbulent eddies[6,13–15]. This is a different mechanism from what is known as 'inertial filtering'[4,9,10,16], which is associated with differences in acceleration between the fluid and the particles, induced by their density difference. In this sense, the motion experienced by neutral particles can be thought of as reflecting the energy spectrum of the turbulence, excluding the scales above a cutoff wavenumber of order inverse the size of the particles. This filtering of the turbulence has differing impacts on different turbulent statistics, as will be seen. For example, quantities whose values are determined by the high-wavenumber tail of the spectrum, such as the dissipation rate of turbulent kinetic energy (TKE) or flow acceleration, if evaluated

[a)] Corresponding author: m.a.teixeira@reading.ac.uk

from the energy spectrum of the particle motion, are necessarily more severely underestimated than quantities whose main contributions come from lower wavenumbers, such as the flow velocity or the integral length scale.

Possible ways of evaluating these filtering effects on finite-sized neutrally-buoyant particles are by performing laboratory experiments of turbulent flows[6,11,17], direct numerical simulations (DNS)[10,15,18,19] or Smoothed Particle Hydrodynamics (SPH) simulations[20], and comparing the statistics of the motion of finite-sized particles with those of tracer particles (with sizes of order the Kolmogorov microscale). This is technically challenging and costly in laboratory experiments, requiring sophisticated particle tracking techniques, and is also challenging using DNS, primarily because it is difficult to attain sufficiently high Reynolds numbers with an accurate representation of the motion of both the fluid and the particles. A simple alternative, despite its inherent limitations, is to assume analytical energy spectra for the turbulence and evaluate the effect of the particles on the fluid motion as a spatial filtering process. That approach, adopted in the present study, follows Lien *et al.*[13] and Lien and D'Asaro[14], and is fundamentally different (and simpler) from the approach used in the stochastic model of Sawford[21].

In order to estimate filtering by the particles of, for example, the dissipation rate and the flow acceleration simultaneously, it is necessary to consider energy spectra both in the wavenumber and in the frequency domain, which must be connected in some way[13,22]. This approach has the advantage of shedding light into a number of fundamental, but not totally clarified, issues in turbulence theory, such as the scaling of the fluid accelerations[23–26], particle accelerations[6,7,15,17], the value of the coefficient scaling the frequency energy spectrum (and the second-order velocity structure function)[27–30], and the variation of these quantities with the Reynolds number. The present work also clarifies how the frequency energy spectrum of the turbulence is related to the wavenumber energy spectrum.

It should be stressed that the results to be presented only apply to isolated neutrally-buoyant particles, and, consistently, in all the datasets considered, the density of the particles never differs from that of the fluid by more than 6%, and their distribution is sparse. Sampling bias effects caused by the preferential concentration of particles in certain flow regions, a phenomenon which is especially important for, but not limited to, non-neutral particles[10,31] is ignored in the theoretical treatment. That is, the particles are assumed to be homogeneously randomly distributed. This is a convenient simplification, but both its implicit use in a previous study[13] and the successful calibration of the present model seem to justify it.

This paper is organised as follows: Sec. II explains the methodology, in particular the adopted wavenumber and frequency energy spectra, and the constraints they must fulfil. Sec. III presents a calibration of the theoretical model, including comparisons of the adopted spectra with available data for the fluid motion and motion of neutrally-buoyant suspended macroscopic particles. Then, in Sec. IV, the impact of particle filtering on the velocity variance, dissipation and acceleration of the fluid estimated from the particles is evaluated. Finally, in Sec. V, a summary of the main conclusions is presented.

## II. METHODOLOGY

### A. Description of the fluid motion

To ensure consistency of the results to be presented, it is necessary to statistically characterise turbulence both in space and in time. Homogeneous and isotropic turbulence will be assumed, as this is the paradigm against which more complicated types of turbulence may be compared. It is likely that the results can be applied with minor alterations to those more complicated types of turbulence. For maximum consistency, most comparisons with experimental or DNS data will also be for homogeneous and isotropic turbulence.

Following Teixeira and Belcher[32], the wavenumber energy spectrum is assumed to take the form

$$E(k) = q^2 l \frac{g_2 (kl)^4}{[g_1 + (kl)^2]^{17/6}} \exp\left[-\frac{3}{2}\alpha(k\eta)^{4/3}\right], \quad (1)$$

where $q$ is the root-mean-square (RMS) velocity of the turbulence, $l$ is the longitudinal integral length scale of the turbulence, $k$ is the wavenumber magnitude, $\alpha$ is the Kolmogorov constant, $\eta$ is the Kolmogorov spatial microscale, and $g_1$ and $g_2$ are dimensionless coefficients dependent on the Reynolds number. The RMS velocity $q$ is defined as $\langle u_i^2 \rangle^{1/2}$ (with $i = 1, 2, 3$), where $u_i$ is turbulent velocity component along the $x_i$ spatial direction and the brackets denote ensemble averaging. The spectrum of Eq. (1), which is assumed here to be a good approximation to real wavenumber energy spectra, can be viewed as a variation of the Corrsin-Pao spectrum[33,34]. It is a blend of a Von Kármán spectrum at low wavenumbers[35] and the exponential tail at high wavenumbers expressed by Eq. (8.4.6) of Tennekes and Lumley[33]. This exponential tail, which delimits the spectrum at high wavenumbers $k_d = O(1/\eta)$, is a finite Reynolds number effect.

The velocity variance, which is the square of the RMS velocity $q$, can also be defined in terms of Eq. (1) as

$$\frac{3}{2}q^2 = \int_0^{+\infty} E(k) dk. \quad (2)$$

The longitudinal integral length scale of the turbulence $l$ is defined as

$$l = \frac{1}{q^2}\int_0^{+\infty} \langle u_1(x_1, x_2, x_3) u_1(x_1 + r_1, x_2, x_3)\rangle dr_1 = \frac{\pi}{2q^2}\int_0^{+\infty} \frac{E(k)}{k} dk, \quad (3)$$

where $(x_1, x_2, x_2)$ is the position and $r_1$ is a spatial lag in the $x_1$ direction. The dissipation rate is given by

$$\varepsilon = 2\nu \int_0^{+\infty} k^2 E(k) dk, \tag{4}$$

where $\nu$ is the kinematic viscosity of the fluid. The integral in Eq. (4) converges appropriately, given the form of $E(k)$.

$E(k)$ can be made dimensionless as $E'(k') = E(k)/(q^2 l)$, in which case Eq. (1) can be expressed in dimensionless form as

$$E'(k') = \frac{g_2 k'^4}{(g_1 + k'^2)^{17/6}} \exp\left(-\frac{45}{2}\alpha Re_\lambda^{-2} \varepsilon'^{-4/3} k'^{4/3}\right), \tag{5}$$

where $k' = kl$, $\varepsilon' = \varepsilon l/q^3$ and $Re_\lambda = q\lambda/\nu$ is the Taylor microscale Reynolds number. Here, the definitions of the Taylor microscale $\lambda = (15\nu q^2/\varepsilon)^{1/2}$, and of the Kolmogorov microscale, $\eta = (\nu^3/\varepsilon)^{1/4}$, as well as the relation $ql/\nu = (1/15)\varepsilon' Re_\lambda^2$, have been used. $E'(k')$ is shown as the black line in Fig. 1(a). Assuming that $\alpha$ and $Re_\lambda$ are prescribed, Eq. (5) has three unknowns: $g_1$, $g_2$ and $\varepsilon'$. These three quantities can be determined using the dimensionless versions of Eqs. (2)-(4), which can be expressed as

$$\int_0^{+\infty} E'(k') dk' = \frac{3}{2}, \tag{6}$$

$$\int_0^{+\infty} \frac{E'(k')}{k'} dk' = \frac{2}{\pi}, \tag{7}$$

and

$$\int_0^{+\infty} k'^2 E'(k') dk' = \frac{1}{30} Re_\lambda^2 \varepsilon'^2. \tag{8}$$

This follows the procedure outlined in Teixeira and Belcher[32]. Solving Eqs. (6)-(8) using Eq. (5) requires employing a root-finding algorithm. Here, a Newton method is used for finding the 3 roots simultaneously. The input parameters are $\alpha$ (supposedly a constant), and $Re_\lambda$. This procedure allows obtaining $\varepsilon'$ (as well as $g_1$ and $g_2$) as a function of $Re_\lambda$, which is thought to be a universal relation in homogeneous and isotropic turbulence[36–38].

For the purpose of estimating fluid accelerations, a Lagrangian frequency energy spectrum $\phi(\omega)$, where $\omega$ is the frequency, is necessary. This is assumed to take the form

$$\phi(\omega) = \frac{\beta\varepsilon}{\omega_0^2 + \omega^2}, \tag{9}$$

for $\omega < \omega_d$ and to be zero otherwise, where $\beta$ and $\omega_0$ are coefficients to be determined. $\omega_d$ is a cutoff frequency due to viscosity and is expected to be $\propto k_d^{2/3}$ if the spectrum has an inertial subrange[33]. Equation (9) is often known as a Lorenz spectrum[2,28]. As shown in Fig. 1(b) (black line), it has the advantage of approaching a constant at low frequencies and decaying as $\omega^{-2}$ at high frequencies (in the inertial subrange), which are features supported both by scaling[39] and observations[2]. Confirmation of the $\omega^{-2}$ decay law has however proved to be challenging in laboratory experiments, and especially so in numerical simulations[30,40], because of the limited extent of the inertial subrange in the frequency domain. Another aspect that has not been clarified sufficiently is how this spectrum decays at frequencies near the dissipation range[33], so an abrupt cutoff at $\omega = \omega_d$ is adopted as the best possible choice. The coefficient $\beta$ is also sometimes named 'Kolmogorov constant' (not to be confused with $\alpha$), but it actually varies with the Reynolds number, as will be seen. It is related to the coefficient $C_0$ to which the second-order structure function of the turbulent velocity is proportional in the inertial subrange (cf. Monin and Yaglom[39], Eq. (21.30')), satisfying $\beta = C_0/\pi$. Two constraints are necessary to define $\beta$ and $\omega_0$ in Eq. (9), and

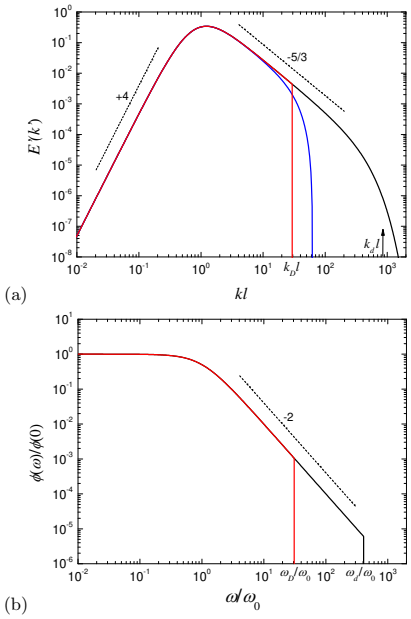


FIG. 1. (a) Wavenumber energy spectrum $E(k)$ (Eq. (5)). Black line: Full spectrum ($k_d \sim 1/\eta$ is the viscous cutoff wavenumber); blue line: spectrum multiplied by Eq. (24), to take into account truncation by finite-sized particles of diameter $D$; red line: approximation of this truncation by an equivalent cutoff wavenumber $k_D \sim 1/D$. (b) Frequency energy spectrum $\phi(\omega)$ (Eq. (9)) normalised by its value at $\omega = 0$. Black line: Full spectrum, with a viscous cutoff at frequency $\omega_d$; red line: spectrum truncated by the particle effect, with a cutoff frequency $\omega_D$. See text for definitions. Dotted lines indicate important power laws.

one additional constraint to define the cutoff frequency $\omega_d$.

The Lagrangian frequency spectrum $\phi(\omega)$ is defined such that

$$q^2 = \int_0^{+\infty} \phi(\omega) d\omega. \tag{10}$$

Note that, in this case, and in contrast with Eq. (2), no factor of 3/2 is present. This follows the convention defined by Tennekes and Lumley[33]. The Lagrangian integral time scale, on the other hand, is defined as

$$T_L = \frac{1}{q^2} \int_0^{+\infty} \langle u_i(t) u_i(t+\tau) \rangle d\tau = \frac{\pi}{2q^2} \phi(0), \tag{11}$$

where $t$ is time, $\tau$ is a time lag, the velocity in the integrand of Eq. (11) is evaluated following fluid parcels, and no summation over the index $i$ is implied. As the viscous cutoff wavenumber of the wavenumber energy spectrum $E(k)$ is of order $1/\eta$, it is both supported by physical reasoning and dimensional analysis[28,33,41], and by laboratory measurements and DNS data[3,18,22], that the cutoff frequency of $\phi(\omega)$ is inversely proportional to the Kolmogorov temporal microscale, $\tau_\eta = (\nu/\varepsilon)^{1/2}$, namely

$$\omega_d = a \left( \frac{\varepsilon}{\nu} \right)^{1/2} \quad \Rightarrow \quad \frac{\omega_d l}{q} = \frac{a}{\sqrt{15}} \varepsilon' Re_\lambda, \tag{12}$$

where $a$ is an adjustable dimensionless constant. Equations (10)-(12) provide sufficient constraints to entirely define Eq. (9). However, the Lagrangian integral time scale $T_L$ further requires a closure assumption. It makes sense physically, and is supported by previous studies[1,3,42,43], that $T_L$, which can be understood physically as an 'eddy turn-over time', is proportional to $l/q$, namely

$$T_L = C \frac{l}{q}, \tag{13}$$

where $C$ is a proportionality coefficient of $O(1)$. Actually, $C$ does not have to be a constant, but, like many other parameters in turbulence theory, it is expected to approach a constant at high $Re_\lambda$. It will be empirically assumed that

$$C = C_\infty \left( 1 + \gamma Re_\lambda^{-1/2} \right), \tag{14}$$

with $C_\infty$ and $\gamma$ being adjustable constants. Although the exact variation of $C$ with $Re_\lambda$ has not been established, it is agreed among a number of authors[1,21,42] that $C$ decreases towards an asymptotic value $C_\infty$ as $Re_\lambda$ increases.

From Eqs. (9), (11) and (13), it can be deduced that

$$\beta = \frac{2}{\pi} C \varepsilon'^{-1} \left( \frac{\omega_0 l}{q} \right)^2. \tag{15}$$

On the other hand, inserting Eq. (9) into Eq. (10), using Eq. (15) and noting that $\phi(\omega) = 0$ for $\omega > \omega_d$, implies that

$$\arctan \left( \frac{\frac{\omega_{d1} l}{q}}{\frac{\omega_0 l}{q}} \right) = \frac{\pi}{2C} \left( \frac{\omega_0 l}{q} \right)^{-1}, \tag{16}$$

where (in accordance with Eq. (12)) $\omega_{d1} = a_1 (\varepsilon/\nu)^{1/2}$ has been defined as the upper limit of integration in $\omega$ for $\phi(\omega)$ (with $a_1$ being an adjustable constant of $O(1)$).

Equations (15)-(16) are equivalent to Eq. (2) of Lien and D'Asaro[28]. Given prescribed values of $C$ (provided by Eq. (14)) and $\omega_{d1} l/q$ (provided by Eq. (12) with $\omega_d = \omega_{d1}$ and $a = a_1$), Eq. (16) may be solved for $\omega_0 l/q$ using a root-finding algorithm, the solution of which is then used in Eq. (15) to obtain $\beta$. A relevant limit is $Re_\lambda \to \infty$. In that case, since from Eq. (12), $\omega_{d1} l/q = a_1/\sqrt{15} \varepsilon' Re_\lambda$, then $\omega_{d1} l/q \to \infty$. Hence Eq. (16) simplifies to $\omega_0 l/q = 1/C_\infty$ and Eq. (15) becomes

$$\beta = \frac{2}{\pi C_\infty} \varepsilon'^{-1}. \tag{17}$$

The flow acceleration is a key quantity in turbulent flows, being filtered by finite-sized particles in a way that will be analysed later. As a departure point, the acceleration of the fluid, or of infinitely small (tracer) particles, which behave essentially like the fluid itself, must be considered. It is well-known (Monin and Yaglom[39], Eq. (21.51)) that the variance of the flow acceleration scales at high $Re_\lambda$ as

$$\langle a_f^2 \rangle \propto \varepsilon^{3/2} \nu^{-1/2} \propto \varepsilon^{4/3} \eta^{-2/3}, \tag{18}$$

where coefficients of proportionality of $O(1)$ are implied. This scaling will be confirmed and extended, not only for high, but also for arbitrary $Re_\lambda$, based on the spectral approach developed here. The acceleration variance for a velocity component can be defined in terms of the Lagrangian frequency spectrum $\phi(\omega)$ as

$$\begin{aligned} \langle a_f^2 \rangle &= \int_0^{+\infty} \omega^2 \phi(\omega) d\omega \\ &= \beta \varepsilon \omega_{d2} \left[ 1 - \frac{\omega_0}{\omega_{d2}} \arctan \left( \frac{\omega_{d2}}{\omega_0} \right) \right], \end{aligned} \tag{19}$$

where (9) has been used, and a cutoff frequency $\omega_{d2} \neq \omega_{d1}$ (defined in accordance with Eq. (12) for $\omega_d = \omega_{d2}$ and $a = a_2$) has been assumed in the integral (with $a_2$ being an adjustable constant). It is expected that $\omega_{d2} > \omega_{d1}$ (and therefore $a_2 > a_1$) due to the fact that $\langle a_f^2 \rangle$ (i.e. the integral of $\omega^2 \phi(\omega)$) receives larger contributions from the viscous tail of spectrum (not explicitly represented) than $q^2$ (i.e. the integral of $\phi(\omega)$). This aspect will be discussed further in Sec. III when $a_1$ and $a_2$ are estimated. Using the definition of $\omega_{d2}$, Eq. (19) can be rewritten as

$$\langle a_f^2 \rangle = a_2 \beta \varepsilon^{4/3} \eta^{-2/3} \left[ 1 - \frac{\omega_0 l/q}{\omega_{d2} l/q} \arctan \left( \frac{\omega_{d2} l/q}{\omega_0 l/q} \right) \right]. \tag{20}$$

The second term inside the square brackets in Eq. (20) is clearly a finite $Re_\lambda$ effect, because it approaches zero as $Re_\lambda \to \infty$ (or $\omega_{d2} \to \infty$), since from Eq. (12) $\omega_{d2} l/q = a_2/\sqrt{(15)}\varepsilon' Re_\lambda$. This shows indeed that $\langle a_f^2 \rangle$ scales as described in Eq. (18). At high $Re_\lambda$, using Eq. (17), Eq. (20) reduces to

$$\langle a_f^2 \rangle = \frac{2a_2}{\pi C_\infty} \varepsilon'^{-1} \varepsilon^{4/3} \eta^{-2/3}. \tag{21}$$

It is worth noting that, in this limit, $\varepsilon'$ approaches a constant value, so the scaling of Eq. (18) remains valid. The scaled acceleration variance $a_0 = \langle a_f^2 \rangle / (\varepsilon^{4/3} \eta^{-2/3})$, which is often known as the Heisenberg-Yaglom coefficient, is expected to be a universal function of $Re_\lambda$ for homogeneous and isotropic turbulence.

This finishes the characterisation of the fluid flow. Next, the motion of finite-sized neutrally-buoyant fluid particles suspended in the flow is described.

### B. Description of the particle motion

It will be considered here that the motion of finite-sized particles is affected only by filtering of spatial scales, neglecting any other effects. This is clearly a simplification, but a meaningful one, given the leading-order importance of this effect[13]. The motion of a spherical particle of diameter $D$ filters all scales of motion in the turbulence that have wavelengths shorter than $D$, but it is possible to be more specific.

Consider a sinusoidal wave of amplitude $A$ and wavenumber $k$, expressing a velocity fluctuation associated with turbulent motion in the $x_3$ direction along the $x_1$ direction:

$$u_3(x_1) = A \cos(k x_1). \tag{22}$$

In order to evaluate how the amplitude of this motion is 'perceived' by a particle of diameter $D$, the value of $u_3$ around $x_1 = 0$ must be averaged over a length $D$ in the $x_1$ direction, namely the smoothed maximum of the filtered cosine wave is given by

$$\frac{1}{D} \int_{-D/2}^{+D/2} A \cos(k x_1) dx_1 = \frac{2A}{kD} \sin\left(\frac{kD}{2}\right), \tag{23}$$

for $kD \leq 2\pi$. This gives the amplitude of the velocity filtered by the particle. This amplitude equals the original unfiltered amplitude $A$ multiplied by the function $2/(kD)\sin(kD/2)$. Since this function approaches 1 as $kD \to 0$, particles with diameters much smaller than $1/k$ do not filter the fluid motion appreciably. If $D \geq O(1/k)$, however, the motion will be attenuated substantially. Since the spectrum is proportional to the square of the amplitude, in order to take this effect into account, the wavenumber energy spectrum of the turbulence $E(k)$ (Eq. (1)) must be multiplied by

$$\left(\frac{2}{kD}\right)^2 \sin^2\left(\frac{kD}{2}\right). \tag{24}$$

This is equivalent to the choice made by Lien *et al.*[13] to represent the effect of filtering of the energy spectrum by buoys in their oceanic measurements (their Eqs. (5.6)-(5.7)). Underlying these choices is the assumption that the particles are, not only neutrally buoyant, but also sparsely distributed, i.e. they have a small volume fraction (which is the case in all of the datasets to be considered). Multiplication of Eq. (1) by Eq. (24) is equivalent to the introduction of a new high-wavenumber tail to the spectrum occurring at wavenumbers substantially lower than $1/\eta$, which limits the energy in the spectrum (and other quantities, such as the dissipation rate) as described by the particles. It will be seen later that this filtering effect can be approximated accurately by ignoring the multiplicative factor Eq. (24) and defining instead an abrupt cutoff at a prescribed wavenumber $k = k_D = O(1/D)$. Namely, the velocity variance probed by the particles $q_p^2 = \langle u_{pi}^2 \rangle$ (defined by analogy with $q^2$, where $u_{pi}$ is the particle velocity in the $i$ direction) is given by

$$\begin{aligned} \frac{3}{2} q_p^2 &= \int_0^{2\pi/D} E(k) \left(\frac{2}{kD}\right)^2 \sin^2\left(\frac{kD}{2}\right) dk \\ &\approx \int_0^{k_D} E(k) dk = \int_0^{k_D l} E'(k') dk', \end{aligned} \tag{25}$$

and the dissipation rate of TKE is given by

$$\begin{aligned} \varepsilon_p &= 2\nu \int_0^{2\pi/D} k^2 E(k) \left(\frac{2}{kD}\right)^2 \sin^2\left(\frac{kD}{2}\right) dk \\ &\approx 2\nu \int_0^{k_D} k^2 E(k) dk = 2\nu \int_0^{k_D l} k'^2 E'(k') dk'. \end{aligned} \tag{26}$$

$E'(k)$ multiplied by $(2/kD)^2 \sin^2(kD/2)$ and $E'(k)$ truncated at wavenumber $k_D$ are shown as the blue and red lines in Fig. 1(a). Equations (25) and (26) are equivalent to Eqs. (2) and (4), but in a truncated form.

Representing the particle filtering effect in the frequency domain requires establishing a relation between frequency and wavenumber, i.e. a kind of 'dispersion relation'. Being a nonlinear phenomenon with strong interactions between different scales, turbulence does not satisfy a dispersion relation, except in a fuzzy sense[13]. However, in the inertial subrange, an approximate relation between the frequency and wavenumber is believed to take the form $\omega \propto \varepsilon^{1/3} k^{2/3}$ (Ref. 33). This was established using dimensional analysis, and can be shown to be required for consistency between the forms of the wavenumber and frequency energy spectra, $E(k)$ and $\phi(\omega)$, in the inertial subrange[33]. Note that this assumption fails when the particle sizes either approach the integral length scale of the turbulence $l$ or the Kolmogorov microscale $\eta$, as those scales fall outside the inertial subrange. Assuming that the particles sizes fall into the inertial subrange of the energy spectrum, and that the cutoff wavenumber due to filtering by the particles is $k_D$, the corresponding cutoff frequency $\omega_D$ should be given by

$$\omega_D = b \varepsilon^{1/3} k_D^{2/3}$$

$$\Rightarrow \quad \frac{\omega_D l}{q} = \frac{b}{\sqrt{15}}\varepsilon' Re_\lambda (k_D D)^{2/3}\left(\frac{D}{\eta}\right)^{-2/3}, \quad (27)$$

where $b$ is a dimensionless constant of $O(1)$. $\phi(\omega)$ truncated at frequency $\omega_D$ is denoted by the red line in Fig. 1(b). For the reasons explained above, $k_D$ is inversely proportional to $D$, i.e. $k_D D$ is a constant. Hence, $k_D D$ is isolated in the second equality of Eq. (27). For similar reasons as pointed out for $\omega_{d1}$ and $\omega_{d2}$, two different values of this cutoff frequency $\omega_D$ need to be defined for the integrals of $\phi(\omega)$ ($\equiv q_p^2$) and of $\omega^2\phi(\omega)$ ($\equiv \langle a_p^2\rangle$), because of the different weights that high frequencies from the spectral tail have on these two integrals near their upper limits. These cutoff frequencies are defined as $\omega_{D1} = b_1\varepsilon^{1/3}k_D^{2/3}$ (i.e. Eq. (27) for $\omega_D = \omega_{D1}$ and $b = b_1$) and $\omega_{D2} = b_2\varepsilon^{1/3}k_D^{2/3}$ (i.e. Eq. (27) for $\omega = \omega_{D2}$ and $b = b_2$), with $b_2 > b_1$. This aspect will be discussed further in Sec. III, when $b_1$ and $b_2$ are estimated.

It is now possible to define the velocity variance $q_p^2$ and the acceleration variance $\langle a_p^2\rangle$ associated with the particle motion, in which the integral of the frequency spectrum $\phi(\omega)$ is only calculated up to the cutoff frequencies $\omega_{D1}$ and $\omega_{D2}$, respectively, namely:

$$q_p^2 = \int_0^{\omega_{D1}} \phi(\omega)d\omega = \frac{\beta\varepsilon}{\omega_0}\arctan\left(\frac{\omega_{D1}}{\omega_0}\right), \quad (28)$$

and

$$\langle a_p^2\rangle = \beta\varepsilon\omega_{D2}\left[1 - \frac{\omega_0}{\omega_{D2}}\arctan\left(\frac{\omega_{D2}}{\omega_0}\right)\right]. \quad (29)$$

Using the definition of $\omega_{D2}$, Eq. (29) can be expressed in the more convenient form:

$$\begin{aligned}\langle a_p^2\rangle &= b_2\beta\varepsilon^{4/3}D^{-2/3}(k_D D)^{2/3} \\ &\quad\times\left[1 - \frac{\omega_0 l/q}{\omega_{D2} l/q}\arctan\left(\frac{\omega_{D2} l/q}{\omega_0 l/q}\right)\right] \\ &= b_2\beta\varepsilon^{4/3}\eta^{-2/3}(k_D D)^{2/3}\left(\frac{D}{\eta}\right)^{-2/3} \\ &\quad\times\left[1 - \frac{\omega_0 l/q}{\omega_{D2} l/q}\arctan\left(\frac{\omega_{D2} l/q}{\omega_0 l/q}\right)\right]. \quad (30)\end{aligned}$$

Equation (30) shows that $\langle a_p^2\rangle/(\varepsilon^{4/3}\eta^{-2/3})$ is a function of $Re_\lambda$ (primarily through $\omega_{D2}l/q$ and $\beta$), $D/\eta$ and $k_D D$. Since $k_D D$ is an adjustable parameter that arises due to the adoption of the cutoff frequency, only $Re_\lambda$ and $D/\eta$ are physically relevant. If $\omega_{D2} \gg \omega_0$, the second term inside the square brackets in Eq. (30) becomes insignificant, and that equation approaches

$$\langle a_p^2\rangle = b_2\beta(k_D D)^{2/3}\varepsilon^{4/3}D^{-2/3}. \quad (31)$$

This means that the particle acceleration variance scales as $\varepsilon^{4/3}D^{-2/3}$, which has indeed been found in a number of studies[6,7]. This supports the legitimacy of assuming Eq. (27), and reveals a possible way of obtaining the scaling of particle accelerations as a function of their diameter.

The principal aim of this study is to systematically show how filtering of the fluid motion by finite-sized particles explains the different underestimations of some key turbulence statistics, such as the velocity variance, the dissipation rate and acceleration variance. One possible way to show the filtering effect of the turbulence properties by the particles is to consider the ratios of those properties probed by the particles to their fluid counterparts. Using wavenumber energy spectra, $E(k)$, the ratio of the velocity variance of the particles to that of the fluid, $q_p^2/q^2$, is given by the ratio of Eq. (25) to Eq. (2), and the corresponding ratio of the dissipation rates, $\varepsilon_p/\varepsilon$, is given by the ratio of Eq. (26) to Eq. (4). Note that the integrals involved in these expressions must be evaluated numerically. Alternatively, in the frequency domain, $q_p^2/q^2$ is given by the ratio of Eq. (28) to Eq. (10), which can be expressed as

$$\frac{q_p^2}{q^2} = \frac{\arctan\left(\frac{\omega_{D1} l/q}{\omega_0 l/q}\right)}{\arctan\left(\frac{\omega_{d1} l/q}{\omega_0 l/q}\right)}, \quad (32)$$

and the ratio of the acceleration variances, $\langle a_p^2\rangle/\langle a_f^2\rangle$, is given by the ratio of Eq. (30) to Eq. (20), which can be expressed as

$$\begin{aligned}\frac{\langle a_p^2\rangle}{\langle a_f^2\rangle} &= \frac{b_2}{a_2}(k_D D)^{2/3}\left(\frac{D}{\eta}\right)^{-2/3} \\ &\quad\times\frac{1 - \frac{\omega_0 l/q}{\omega_{D2} l/q}\arctan\left(\frac{\omega_{D2} l/q}{\omega_0 l/q}\right)}{1 - \frac{\omega_0 l/q}{\omega_{d2} l/q}\arctan\left(\frac{\omega_{d2} l/q}{\omega_0 l/q}\right)}. \quad (33)\end{aligned}$$

Equations (32) and (33) are only valid under the assumptions that $\omega_{D1} < \omega_{d1}$ and $\omega_{D2} < \omega_{d2}$, which ensure that $q_p^2/q^2 \le 1$ and $\langle a_p^2\rangle/\langle a_f^2\rangle \le 1$. When both $Re_\lambda \gg 1$ and $\omega_{D2} \gg \omega_0$, Eq. (33) reduces to

$$\frac{\langle a_p^2\rangle}{\langle a_f^2\rangle} = \frac{b_2}{a_2}(k_D D)^{2/3}\left(\frac{D}{\eta}\right)^{-2/3}. \quad (34)$$

Additionally, the definitions of $q_p^2$ from $E(k)$ or $\phi(\omega)$ (Eq. (25) or Eq. (28)), and therefore those of $q_p^2/q^2$ (ratio of Eq. (25) to Eq. (2), or Eq. (32)) should, of course, coincide.

This completes the description of the methodology. The model summarised by Eqs. (32)-(33) will be calibrated next against laboratory and DNS data to determine the best-fitting constants $a_1$, $a_2$, $b_1$, $b_2$, $C_\infty$, $\gamma$ and $k_D D$ (which are initially free parameters), and then used to estimate the filtering effects on $q^2$, $\varepsilon$ and $\langle a_f^2\rangle$ by the particles.

## III. CALIBRATION OF THE MODEL

### A. Turbulent flow statistics

A first test to the model developed in Sec. II-A is provided by how well it is able to predict the variation of

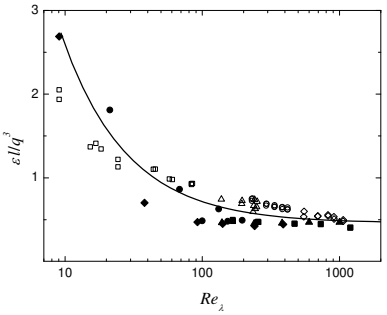


FIG. 2. Variation of $\varepsilon'$ with $Re_\lambda$. Symbols: data from Fig. 4 of Djendi *et al.*[38], predominantly for homogeneous and isotropic turbulence, but also including data from jets and grid-generated turbulence. Open symbols: laboratory experiments; filled symbols: DNS data; line: prediction from Eqs. (5)-(8) with $\alpha = 2$.

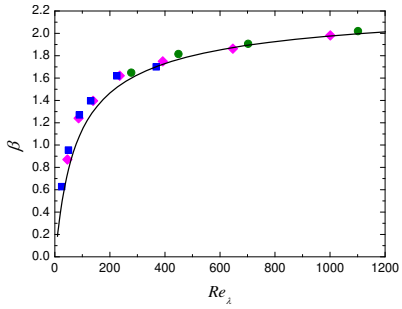


FIG. 3. Variation of $\beta$ with $Re_\lambda$ for homogeneous and isotropic turbulence. Symbols: DNS data from Fig. 2(c) of Barjona and da Silva[30] (symbols as similar as possible to those used in the original figure); line: prediction from Eqs. (14)-(16), for $a_1 = 0.8$, $C_\infty = 0.58$ and $\gamma = 5$.

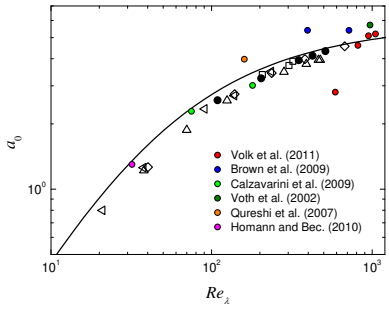


FIG. 4. Variation of the Heisenberg-Yaglom coefficient $a_0$ as a function of $Re_\lambda$ for homogeneous and isotropic turbulence. Black and white symbols: data from Fig. 7 of Lawson *et al.*[26] (symbols as similar as possible to those used in the original figure); colour symbols: data from various experimental and DNS datasets (see legend and Table I); line: model prediction from Eq. (20) along with Eqs. (14)-(16) and (12), for $a_1 = 0.8$, $a_2 = 2.5$, $C_\infty = 0.58$ and $\gamma = 5$.

$\varepsilon'$ with $Re_\lambda$. Figure 2 shows this relationship, from 18 separate datasets (some resulting from laboratory experiments, others from DNS, most of them for homogeneous and isotropic turbulence) included in Fig. 4 of Djendi *et al.*[38] (symbols), and as predicted by the spectrum $E'(k')$ of Eq. (5) subject to the constraints Eqs. (6)-(8) (line). In Eq. (5), it was assumed that $\alpha = 2$, as in Teixeira and Belcher[32], which ensures that $\varepsilon' \approx 0.475$ when $Re_\lambda \to \infty$, as suggested by the data. Although there is substantial scatter in the data, the line roughly follows the trend in the data, increasing at low $Re_\lambda$, as shown by all existing datasets. This agreement gives some confidence in the accuracy of $E(k)$ in Eq. (1) as a suitable wavenumber energy spectrum.

Figure 3 shows the variation $\beta$ with $Re_\lambda$ from various DNS results for homogeneous and isotropic turbulence included in Fig. 2(c) of Barjona and da Silva[30] (symbols) and from Eqs. (14)-(16) (line), for $C_\infty = 0.58$, $\gamma = 5$ and $a_1 = 0.8$. The values of $\beta$ from Barjona and da Silva[30] were obtained from the corresponding $C_0$ for the velocity structure function (mentioned before), so they had to be divided by $\pi$ (see Monin and Yaglom[39], Eq. (21.36)). Assuming that $C$ is a function of the Reynolds number, as described by Eq. (14), turns out to be important for being able to predict well simultaneously the variation of $\beta$ (in Fig. 3) and $\langle a_I^2 \rangle$ (to be shown in Fig. 4) with $Re_\lambda$. The variation of $\beta$ with $Re_\lambda$ shows a relatively fast increase at low values of $Re_\lambda$ and approach to an asymptotic value at high $Re_\lambda$. This is quite well predicted by the model, albeit with some underestimation at low $Re_\lambda$. From Eq. (17) and the fact that $\varepsilon' \approx 0.475$ at high $Re_\lambda$, the asymptotic limit of $\beta$ as $Re_\lambda \to \infty$ is approximately 2.31.

Figure 4 shows the variation of the Heisenberg-Yaglom coefficient, $a_0$, as a function of $Re_\lambda$ for various datasets and the model prediction. The latter is obtained using Eq. (20), assuming $C_\infty = 0.58$, $\gamma = 5$ and $a_1 = 0.8$ (as previously), and $a_2 = 2.5$. Tests made using a Lagrangian frequency spectrum $\phi(\omega)$ that decays $\propto \omega^{-4}$ for $\omega > \omega_d$, as in Sawford[21] (not shown) produced results almost indistinguishable from those in Figs. 3 and 4, only requiring the adjustment of a single constant analogous to $a_1$ and $a_2$. However, this test spectrum produced less satisfactory particle flow statistics, implying that its form needed to be refined further, which is beyond the scope of this study. Nevertheless, these tests show that the different frequency cutoffs $\omega_{d1}$ and $\omega_{d2}$ are a simplified, but valid *ad hoc* representation of the high-frequency tail of $\phi(\omega)$, which is essential to be able to properly fit the data in Figs. 3 and 4. The agreement of the theoretical prediction with the collection of data from Lawson *et al.*[26] in

TABLE I. Source of the datasets used in Figs. 4–8 for comparison with and calibration of the model. In these datasets, $\langle a_p^2 \rangle$ is either normalized by $\varepsilon^{4/3}\eta^{-2/3}$ or by $\langle a_f^2 \rangle$. The dataset of Calzavarini *et al*[16] includes two data subsets by Qureshi *al.*[6] and Voth *et al.*[44]. The dataset of Uhlmann and Chouippe[5] includes a data subset by Yeo *et al.*[45].

| Present figures | Source of data | Figure in source |
|---|---|---|
| Fig. 4 | Lawson *et al.*[26] | Fig. 7 |
| Figs. 4 and 5 | Volk *et al.*[7] | Table 1; Fig. 3 |
| Figs. 4 and 5 | Brown *et al.*[17] | Fig. 2(a) |
| Figs. 4 and 6 | Calzavarini *et al*[16] | Fig. 2 |
| Figs. 4 and 7 | Homann & Bec[19] | Figs. 1(b) and 2(a) |
| Fig. 8 | Uhlmann & Chouippe[5] | Figs. 2 and 5 |

Fig. 4 is good, although the model tends to slightly overestimate the data. The asymptotic value of the scaled acceleration variance for $Re_\lambda \to \infty$ can be shown from Eq. (21) to be 5.78.

The values of $a_0$ from the other datasets, to be used in the next section (see Table 1), also follow the general trend, but show in a few cases a noticeable departure from the theoretical prediction. Without correction, these values of $a_0$ would lead to substantial disagreement between data and the theoretical estimate of $\langle a_p^2 \rangle/(\varepsilon^{4/3}\eta^{-2/3})$, particularly for the case of Volk *et al.*[7] with $Re_\lambda = 590$ (not shown). Given the robust trend of the Lawson *et al.*[26] data and the good agreement with the model prediction, the offset values of $a_0$ were corrected by replacing them with the values predicted by the model at the same $Re_\lambda$ in the rest of the paper. For example, the value $a_0 = 2.8$ proposed by Volk *et al.*[7] at $Re_\lambda = 590$ (see their Table 1) was adjusted to 4.6. The corrected values of $a_0$ will be used in the next section to relate $\langle a_p^2 \rangle/(\varepsilon^{4/3}\eta^{-2/3})$ and $\langle a_p^2 \rangle/\langle a_f^2 \rangle$ in each dataset.

Note that although all theoretical predictions of the variation of $\beta$ and $a_0$ with $Re_\lambda$ provided by previous authors have been empirical fits, with the exception of Lien and D'Asaro[28] for $\beta$[26,30], the present model, despite being slightly less accurate than those fits, provides a physically consistent framework for calculating both quantities, which is new in the case of $a_0$. Crucial to a simultaneously good prediction of $\beta$ and $a_0$ is the value of the coefficient $a_2$, which defines the cutoff frequency for the acceleration variance. As can be seen from Eqs. (17) and (21), the limit of $a_0$ for $Re_\lambda \to \infty$ differs from that of $\beta$ by the factor $a_2$.

### B. Particle motion statistics

The preceding section has calibrated the adopted turbulence model for the fluid flow. The part of the model that concerns the statistics of finite-sized neutrally-buoyant particles suspended in the fluid is now calibrated and tested against laboratory experiments and DNS. Although all of the DNS data selected are for homogeneous and isotropic turbulence, the experimental data include turbulence that may not be perfectly isotropic, owing to the limitations of the (typically Von Kármán or wind tunnel) experimental setups used to generate the turbulence[6,44]. Voth *et al.*[44] noted that the acceleration is much less anisotropic than the velocity in these circumstances, which is not surprising given that the acceleration receives most of its contributions from higher frequencies/wavenumbers. With this in mind, all comparisons of velocity variances will be made here with DNS of homogeneous and isotropic turbulence, whereas both experiments and DNS will be considered for comparisons of the acceleration variance.

Figure 5 shows model predictions together with the experimental datasets of Volk *et al.*[7] and Brown *et al.*[17] for the particle acceleration variance $\langle a_p^2 \rangle$ normalised either by the factor $\varepsilon^{4/3}\eta^{-2/3}$ (Fig. 5(a)) or by the fluid acceleration variance $\langle a_f^2 \rangle$ (Fig. 5(b)), at different Reynolds numbers $Re_\lambda$. In Fig. 5(a), the data from Volk *et al.*[7] in the form $\langle a_p^2 \rangle/\langle a_f^2 \rangle$ were extracted from their Fig. 3 and rescaled by multiplying by the corrected Heisenberg-Yaglom coefficient, $a_0$, whereas the data of Brown *et al.*[17] kept a similar normalization as in their original Fig. 2(a), $\langle a_p^2 \rangle/(\varepsilon^{4/3}\eta^{-2/3})$. In Fig. 5(b), the data from Brown *et al.*[17] in the form $\langle a_p^2 \rangle/(\varepsilon^{4/3}\eta^{-2/3})$ in their Fig. 2(a) were divided by $a_0$, whereas the data of Volk *et al.*[7] kept a similar normalization, $\langle a_p^2 \rangle/\langle a_f^2 \rangle$, as in their original Fig. 3. The model predictions from Eq. (30) and Eq. (33) are shown for $Re_\lambda = 1050$ (solid line) and $Re_\lambda = 396$ (dashed line), which are the upper and lower limits of $Re_\lambda$ considered in these datasets. In Eq. (30), the dependence on the Reynolds number comes almost totally from $\beta$, although a weak dependence also comes from $\omega_0 l/q$. This is corroborated by the fact that in Eq. (33) used in Fig. 5(b) (where $\beta$ does not appear), the dependence on $Re_\lambda$ is very weak.

In Fig. 5(a), the agreement of the model predictions with the data seems very good for a substantial range of $D/\eta$. The turbulence model follows an approximate asymptote $\propto (D/\eta)^{-2/3}$, as shown in the figure and in agreement with Eq. (30). Once $D/\eta$ decreases to values of $O(1)$, however (vertical dotted lines, which correspond to $\omega_{D2} = \omega_{d2}$, or equivalently $D/\eta = (b_2/a_2)^{3/2} k_D D \approx 4.55$), Eqs. (30) and (33) lose their accuracy, overestimating the data, which stabilise to a constant value at low $D/\eta$, corresponding to $a_0$. The reason for this behaviour is that, in the measurements, the particles are reaching sizes that match the exponential tail of the wavenumber energy spectrum $E(k)$ (i.e. they behave like tracers), and so the scaling of the acceleration variance shifts from $\varepsilon^{4/3}D^{-2/3}$ to $\varepsilon^{4/3}\eta^{-2/3}$. The cloud of data to the right of the vertical dotted line falls approximately between the theoretical lines, with data for the highest Reynolds numbers closer to the upper line and data for the lowest Reynolds numbers closer to the lower line, as would be expected. This gives a reassuring indication about

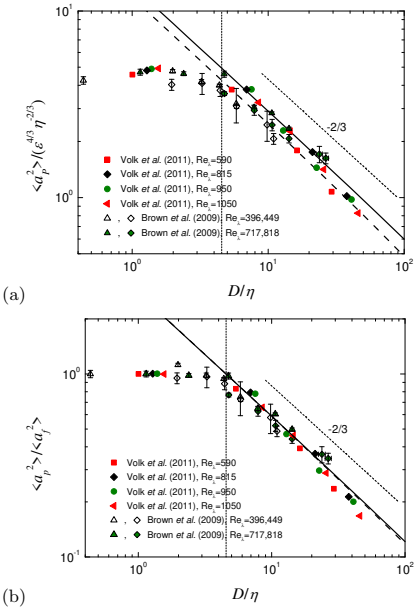


FIG. 5. Variation of the particle acceleration variance $\langle a_p^2\rangle$ as a function of $D/\eta$ for different values of $Re_\lambda$. The model predictions are compared with six experimental datasets using two normalisations: (a) $\langle a_p^2\rangle/(\varepsilon^{4/3}\eta^{-2/3})$, and (b) $\langle a_p^2\rangle/\langle a_f^2\rangle$. Symbols: data from Volk *et al.*[7] and Brown *et al.*[17] (see legend for details); thick lines: predictions from Eqs. (30) and (33), along with Eqs. (14)-(16), (12) and (27), for $a_1 = 0.8$, $a_2 = 2.5$, $b_1 = 0.84$, $b_2 = 3.3$, $C_\infty = 0.58$, $\gamma = 5$ and $k_D D = 3$. Solid lines: $Re_\lambda = 1050$; dashed lines: $Re_\lambda = 396$. Vertical dotted line: $D/\eta = (b_2/a_2)^{3/2} k_D D \approx 4.55$; oblique dotted line: $\propto (D/\eta)^{-2/3}$.

the reliability of the $a_0$ trend displayed by the dataset of Lawson *et al.*[26] and the model prediction in Fig. 4.

In Fig. 5(b), showing $\langle a_p^2\rangle/\langle a_f^2\rangle$, all datasets should approach a value of 1 for $D/\eta \to 0$. This is the case by construction in the original data from Volk *et al.*[7] and also in the data from Brown *et al.*[17] calculated using the values of $a_0$ from Fig. 4. Within the range of $D/\eta$ for which the model is expected to be valid (i.e. the region where $\langle a_p^2\rangle/\langle a_f^2\rangle$ is expected to decay as $(D/\eta)^{-2/3}$ to the right of the vertical dotted line), the agreement between theory and measurements is quite good, with the data almost collapsing to a single line, as predicted.

Figure 6 shows the normalised particle acceleration $\langle a_p^2\rangle/(\varepsilon^{4/3}\eta^{-2/3})$ extracted from Fig. 2 of Calzavarini *et al.*[16] along with the model predictions from Eq. (30) for $Re_\lambda = 75$, 180 and 970. The model prediction for $Re_\lambda = 970$ matches the data subset of Voth *et al.*[44] included in Fig. 2 of Calzavarini *et al.*[16], whereas the

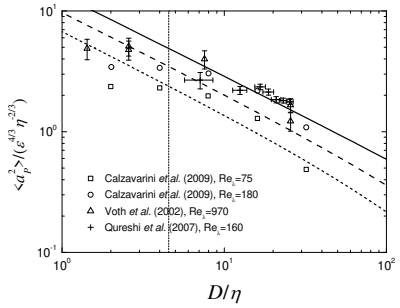


FIG. 6. Variation of the normalised particle acceleration variance $\langle a_p^2\rangle/(\varepsilon^{4/3}\eta^{-2/3})$ as a function of $D/\eta$ for different values of $Re_\lambda$. Symbols: data from Calzavarini *et al.*[16], Voth *et al.*[44] and Qureshi *et al.*[6] (see legend); lines: predictions from Eq. (30), along with Eqs. (14)-(16) and (27), for the same input parameters as used in Fig. 5. Solid line: $Re_\lambda = 970$; dashed line: $Re_\lambda = 180$; dotted line: $Re_\lambda = 75$. Vertical dotted line: $D/\eta = (b_2/a_2)^{3/2} k_D D \approx 4.55$.

other two values of $Re_\lambda$ match those of the DNS of homogeneous and isotropic turbulence of Calzavarini *et al.*[16]. The second data subset of Calzavarini *et al.*[16] from Qureshi *et al.*[6] is also included in Fig. 6. It can be seen in Fig. 6 that although the model predictions slightly underestimate the corresponding data sets in their intermediate range (by a factor of less than about 1.5), the trend with the Reynolds number is correct, except for the data of Qureshi *et al.*[6], which having $Re_\lambda = 160$ should be essentially at the same level as the the DNS data from Calzavarini *et al.*[16] at $Re_\lambda = 180$, whereas the graph shows that it is closer to the the data subset by Voth *et al.*[44] at $Re_\lambda = 970$. The reasons for this discrepancy are unclear. Another aspect worthy of note is that in the DNS of Calzavarini *et al.*[16] there is not a well defined $(D/\eta)^{-2/3}$ asymptotic behaviour. This is probably a consequence of the fact that the Reynolds number is too low, and therefore the inertial subrange in the turbulence is not well developed (this problem is typically much less acute in laboratory experiments).

In their theoretical predictions, Calzavarini *et al.*[12,16] adopt a so-called Faxén approach, part of which consists of extrapolating the behaviour of the acceleration of tracers to finite-sized particles. Although this approximation, which is based on a Taylor series expansion of the acceleration variance around $D/\eta = 0$ (see Fig. 3 of Calzavarini *et al.*[12]), works well for the transition between the tracer and finite-size behaviour of the particles, it naturally fails for larger particles, and is, in particular, unable to capture the $(D/\eta)^{-2/3}$ asymptotic law that relies on the behaviour of the particles in the inertial subrange.

In Fig. 7, data from DNS of homogeneous and isotropic turbulence with $Re_\lambda = 32$ from Homann and Bec[19] for

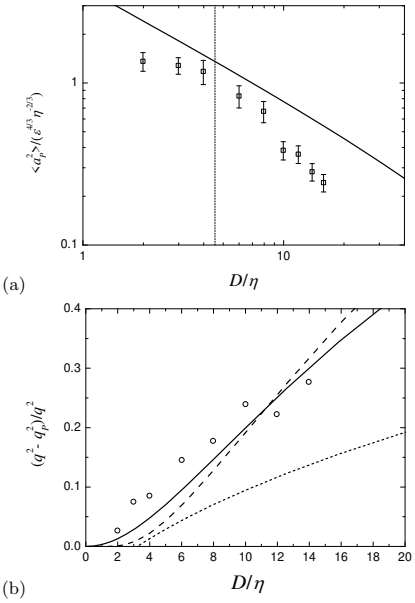


FIG. 7. Variation of the normalised particle acceleration and velocity variance as a function of $D/\eta$ for $Re_\lambda = 32$, in respectively (a) $\langle a_p^2\rangle/(\varepsilon^{4/3}\eta^{-2/3})$, and (b) $(q^2 - q_p^2)/q^2$. Symbols: data from Homann and Bec[19]. In (a) the line comes from Eq. (30) and in (b) the solid and dashed lines come from the first and second equalities of Eq. (25) with $k_D D = 2.2$, and the dotted line comes from Eq. (32). Equations (14)-(16), (12) and (27) are also used, along with the same input parameters as in Fig. 5. Vertical dotted line: $D/\eta = (b_2/a_2)^{3/2} k_D D \approx 4.55$.

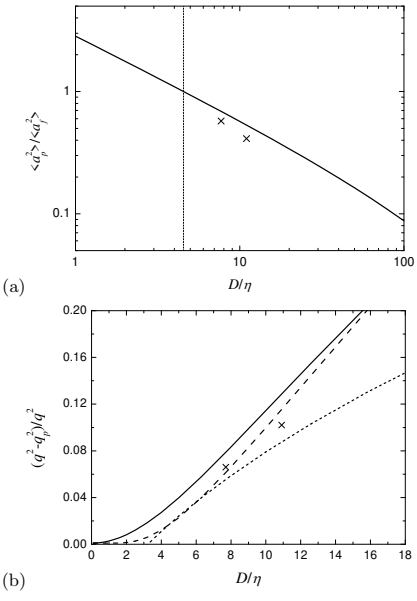


FIG. 8. Variation of the normalised particle acceleration and velocity variance as a function of $D/\eta$ for $Re_\lambda = 58$ in respectively (a) $\langle a_p^2\rangle/\langle a_f^2\rangle$, and (b) $(q^2 - q_p^2)/q^2$. Symbols: data from Yeo *et al.*[45]; lines: predictions from Eqs. (33), (25) and (32), along with Eqs. (14)-(16), (12) and (27), for the same input parameters as in Fig. 5. Vertical dotted line: $D/\eta = (b_2/a_2)^{3/2} k_D D \approx 4.55$. The solid line in (b) shows $q_p^2/q^2$ obtained from the first equality of Eq. (25), the dashed line from the second equality of Eq. (25) (both with $k_D D = 2.2$) and the dotted line from Eq. (32).

$\langle a_p^2\rangle/(\varepsilon^{4/3}\eta^{-2/3})$ and $(q^2 - q_p^2)/q^2 = 1 - q_p^2/q^2$ (adapted from their Figs. 2(a) and 1(b), respectively) are shown, along with predictions from the present model. In Fig. 7(a), the model prediction is from Eq. (30). In Fig. 7(b) the model predictions are based on the non-approximated wavenumber energy spectrum $E(k)$ (first equality of Eq. (25)), the approximated wavenumber energy spectrum (second equality of Eq. (25)), and the frequency energy spectrum $\phi(\omega)$ expressed by Eq. (32). In Fig. 7(a), the trend and order of magnitude of the acceleration variance is reproduced, but the model now overestimates the data slightly (by a factor of about 1.3 at the point where the symbols approach the line most), and the asymptotic behaviour $(D/\eta)^{-2/3}$ is poorly defined, as would be expected for flow with such a low $Re_\lambda$. In Fig. 7(b), the calculation based on the non-truncated wavenumber energy spectrum $E(k)$ reproduces the variation of the velocity variance with $D/\eta$ fairly well; this is achieved less successfully, especially for low $D/\eta$, by the calculation based on the truncated wavenumber energy spectrum, and Eq. (32) underestimates the data by a factor of 2 or more. This is a consequence of the fact that, for very low $Re_\lambda$, Eq. (27) is not a particularly good approximation. However, it will be seen that for higher $Re_\lambda$ the solid, dashed and dotted lines converge, as they should. Provided this happens, the ability of the solid line to predict the trend of the data in Fig. 7(b) is reassuring.

Finally, in Fig. 8 the normalised acceleration variance and velocity variance are shown for the DNS data subset of Yeo *et al.*[45], from Figs. 5 and 2 of Uhlmann and Chouippe[5], for $Re_\lambda = 58$. The agreement between the model prediction and the DNS data for the scaled particle acceleration variance $\langle a_p^2\rangle/\langle a_f^2\rangle$ is clearly predicted satisfactorily, but more interestingly the prediction for the scaled particle velocity variance $(q^2 - q_p^2)/q^2$ for this slightly higher value of $Re_\lambda$ is better than in Fig. 7(b). Both Eq. (25) with a non-truncated wavenumber energy spectrum $E(k)$ and with a truncated spectrum follow the magnitude and trend of the DNS data, but Eq. (32) is

now much closer to the data, showing its convergence with Eq. (25) as $Re_\lambda$ increases.

It should be noted that the values of $b_1 = 0.84$ and $b_2 = 3.3$ adopted throughout this study (see caption of Fig. 5) rely on a good fit of both the velocity and acceleration variances filtered by the particles in Figs. 7 and 8, and ensure that $q_p^2$ based on $E(k)$ and $\phi(\omega)$, shown in Fig. 9a, are consistent. This amounts to extending the spectrum of $\langle a_p^2 \rangle$ to substantially higher frequencies than the spectrum of $q_p^2$ (as was done in Sec. IIIA for $\langle a_f^2 \rangle$ and $q_f^2$ to account for the viscous tail of $\phi(\omega)$). The fact that the disparity between $b_1$ and $b_2$ is comparable to that between $a_1$ and $a_2$ suggests that the decay of $\phi(\omega)$ for $\omega > \omega_D$ is not very different from that for $\omega > \omega_d$. This highlights the limitations of Eq. (27), namely the fact that the relation between $\omega$ and $k$ is nonlocal, and frequencies $\omega > \omega_D$ may receive contributions from wavenumbers $k < k_D$. Hence, a sharp cutoff $k_D$ in $E(k)$ can correspond to a smoother tail in $\phi(\omega)$ beyond $\omega_D$. A similar argument is of course applicable to the viscous cutoff wavenumber $k_d$ and frequency $\omega_d$, and may qualitatively explain the form of the tail of $\phi(\omega) \propto \omega^{-4}$ proposed by Sawford [21].

All of the results presented in this section support the idea that the model developed here is suitably calibrated and can be used to predict how turbulence statistics are filtered by the motion of neutrally-buoyant finite-sized particles, at sufficiently high Reynolds numbers. Those predictions will be provided next.

## IV. FILTERING OF THE PARTICLE MOTION

The way in which filtering of the turbulence energy spectrum by the particles affects the evaluation of statistics calculated based on the particle motion will next be estimated. These statistics are the velocity variance $q^2$, the TKE dissipation rate $\varepsilon$ and the acceleration variance $\langle a_f^2 \rangle$. $\varepsilon$ is intrinsically defined as an integral in the wavenumber domain, and $\langle a_f^2 \rangle$ as an integral in the frequency domain. $q^2$ can be expressed both as an integral in wavenumber and in frequency, as pointed out previously. This redundancy provides a constraint for the estimates of this quantity, which is implicit in the calibration process presented in the preceding section, but will become more explicit here. The accuracy of the acceleration variance estimates is also ensured by the previous calibration process. It is worth noting that, while $q_p^2$ and $\langle a_p^2 \rangle$ are measured directly from the particle motion, $\varepsilon_p$ (and $\varepsilon$) is typically estimated from the velocity spectrum or structure functions compensated by inertial subrange functionals[46–48]). This definition is subject to a potentially smaller error than if it was given by Eq. (4), which may be simply estimated for wavenumber $k$ in the inertial subrange using Eq. (24). However, it is still useful to understand by how much $\varepsilon$ is underestimated using Eq. (4). Additionally, comparing estimates of the filtering of $q^2$ and $\varepsilon$ by particles neatly illustrates how the contribution of the spectral tail to each of these quantities differently affects the definition of their respective viscous cutoff wavenumbers.

Figure 9 shows $q_p^2/q^2$, $\varepsilon_p/\varepsilon$ and $\langle a_p^2 \rangle / \langle a_f^2 \rangle$ as a function of $Re_\lambda$ for particles with different values of the ratio of the particle diameter to the integral length scale of the turbulence, $D/l$. The dependence of the results on $D/l$ as a measure of the finite dimensions of the particles is analysed, because, in a given experimental setup, $D/l$ is more likely to remain fixed as $Re_\lambda$ is varied than $D/\eta$ (for particles of a given size). But results could be equally easily plotted for different $D/\eta$. In Fig. 9(a), the results obtained from the first equality of Eq. (25) can be considered an essentially exact calculation, if the wavenumber energy spectrum $E(k)$ given by Eq. (1) is a good approximation to real spectra and if the effect of the particles is primarily spatial filtering. The model predictions obtained from the second equality of Eq. (25) include a cutoff wavenumber $k_D D = 2.2$ that is applied everywhere in the calculation of $q_p^2$. As can be seen, this approximation is overall quite accurate. The approximation using the frequency spectrum $\phi(\omega)$, Eq. (32), is less accurate, especially for $D/l = 0.5$, but becomes quite accurate for $D/l \leq 0.2$, showing that the assumption expressed by Eq. (27) is sound, as long as $b_1$ is properly estimated. The lower accuracy of Eq. (32) for $D/l > 0.2$ is because the frequency cutoff due to the particle is below the lower frequency end of the inertial subrange, but Eq. (27) is assumed to always apply perfectly. In fact, it would be possible to obtain a perfect agreement between the two approximations by implementing that agreement as a constraint on the formulation of the frequency spectrum model, in which case $b_1$ would become a function of $Re_\lambda$. But that approach would not add much to the physical significance of the model, while increasing its computational complexity.

In general terms, Fig. 9(a) shows that $q_p^2/q^2$ decreases as $D/l$ increases (as is intuitive) and, for each value of $D/l$, decreases as $Re_\lambda$ increases. This is because, for a given $D/l$, a higher value of $Re_\lambda$ corresponds to a larger fraction of the spectrum existing to the right of the spectral cutoff imposed by the particle. This can be understood as follows: it can be shown using the definitions of $\eta$ and $Re_\lambda$ that

$$\frac{\eta}{l} = \frac{\eta}{D}\frac{D}{l} = 15^{3/4}\varepsilon'^{-1} Re_\lambda^{-3/2} \propto Re_\lambda^{-3/2}. \tag{35}$$

So, if $D/l$ is kept fixed, $D/\eta$ increases as $Re_\lambda$ increases. In the experiments of Mériaux *et al.*[8], the adopted neutrally-buoyant particles had a diameter $D = 2.2\,\mathrm{cm}$ and $l \approx 10.2 - 12.1\,\mathrm{cm}$, which gives $D/l \approx 0.2$, and $Re_\lambda$ was estimated to vary between 292 and 418 (see their Table 2). Figure 9(a) suggests that in that case $q_p^2/q^2 \approx 0.8$ which implies that $q_p/q \approx 0.9$. So the flow RMS velocity is little underestimated, despite the fact that $D$ is only 5 times smaller than the integral length scale of the turbulence.

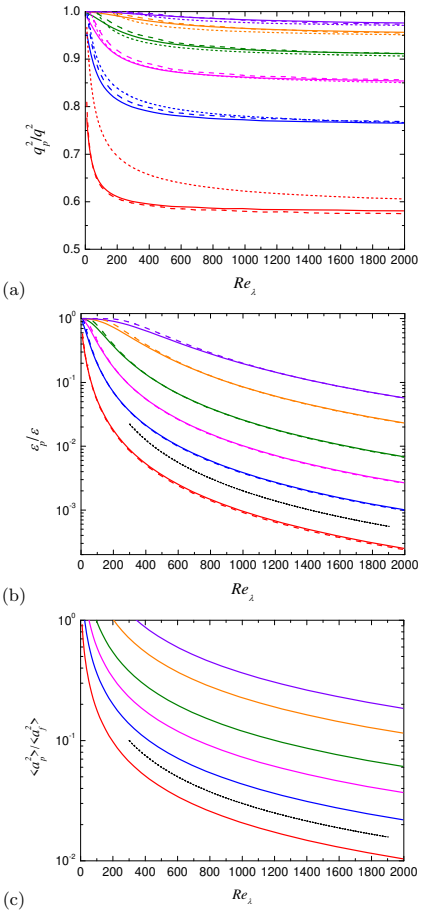


FIG. 9. Ratios of the (a) velocity variances $q_p^2/q^2$, (b) dissipation rates $\varepsilon_p/\varepsilon$ and (c) acceleration variances $\langle a_p^2\rangle/\langle a_f^2\rangle$ obtained from the particle motion to those associated with the fluid motion, as a function of $Re_\lambda$ for different values of $D/l$. Red lines: $D/l = 0.5$, blue lines: $D/l = 0.2$, magenta lines: $D/l = 0.1$, green lines: $D/l = 0.05$, orange lines: $D/l = 0.02$, violet lines: $D/l = 0.01$. Solid lines in (a) and (b): results from the first equalities of Eqs. (25) and (26), respectively. Dashed lines in (a) and (b): results for the second equalities of Eqs. (25) and (26), assuming $k_D D = 2.2$ and $k_D D = 2.9$, respectively. Dotted lines in (a) and solid lines in (c): results from Eqs. (30) and (33), assuming the same input constants as in Fig. 5. The black dotted line in (b) is $\propto Re_\lambda^{-2}$ and that in (c) is $\propto Re_\lambda^{-1}$.

In Fig. 9(b), $\varepsilon_p/\varepsilon$ predicted by the first equality of Eq. (26) can also be considered essentially exact, for the reasons pointed out above. The second equality of Eq. (26), with an abrupt cutoff wavenumber, assumes that $k_D D = 2.9$. Note that this dimensionless cutoff wavenumber is larger than the one applied to calculate $q_p^2/q^2$. This is a manifestation of the larger weight of the spectrum at high wavenumbers in $\varepsilon$ relative to $q^2$, but the difference is smaller than for the cutoff frequencies of $\phi(\omega)$, because the viscous tail of $E(k)$ is exponential. The agreement between the dissipation ratios calculated with the smooth or abrupt cutoff wavenumbers is very good, becoming slightly worse at the lowest values of $D/l$ and $Re_\lambda$. The remarkable difference of Fig. 9(b) relative to Fig. 9(a) is that $\varepsilon_p/\varepsilon$ quickly attains a very small value, of $O(0.1)$ or even $O(0.01)$ for common values of $D/l$ and $Re_\lambda$. It is therefore extremely difficult to estimate $\varepsilon$ accurately from its primary definition using the particle motions, unless these particles are essentially tracers or the Reynolds number is very low. Since $D$, and therefore $k_D$, are related to $l$ by fixed factors, the dependence of $\varepsilon_p/\varepsilon$ on $Re_\lambda$ is due essentially to the dependence of $\varepsilon$ on $Re_\lambda$, which, from integration of Eq. (26) is of the type $\varepsilon \propto k_d^{4/3} \propto Re_\lambda^2$, leading to an asymptotic dependence $\varepsilon_p/\varepsilon \propto Re_\lambda^{-2}$ (black dotted line in the graph). Physically, this can be interpreted as being due to the fact that as $Re_\lambda$ increases the turbulence contains smaller and smaller eddies, which are unreachable by finite-sized particles.

Figure 9(c) shows the dependence of $\langle a_p^2\rangle/\langle a_f^2\rangle$ predicted by Eq. (33). In this case no alternative result is available for comparison, but the calibration carried out in the preceding section should ensure reliability of this result. $\langle a_p^2\rangle/\langle a_f^2\rangle$ increases as $D/l$ decreases, as would be expected, and decreases also with $Re$, in a way that looks qualitatively similar to that for $\varepsilon_p/\varepsilon$ in Fig. 9(b), but the variation with $Re_\lambda$ is weaker. The points where the lines reach $\langle a_p^2\rangle/\langle a_f^2\rangle = 1$ correspond to $\omega_{D2} = \omega_{d2}$, i.e. the vertical lines in Figs. 5-8. As happened for $\varepsilon_p/\varepsilon$ in Fig. 9(b), the dependence of $\langle a_p^2\rangle/\langle a_f^2\rangle$ with $Re_\lambda$ is mostly due to $\langle a_f^2\rangle \propto \omega_{d2} \propto Re_\lambda$ (from Eq. (19)), so that $\langle a_p^2\rangle/\langle a_f^2\rangle \propto Re_\lambda^{-1}$ (black dotted line in the graph). These asymptotic dependences of $\varepsilon_p/\varepsilon$ and $\langle a_p^2\rangle/\langle a_f^2\rangle$ on $Re_\lambda$ result from the general form of the turbulence spectra in the inertial subrange, so they are quite robust, being independent of the details of the present model. Clearly, the acceleration variance is not as attenuated by the particles as the dissipation rate, but $\langle a_p^2\rangle$ can still easily reach 10% of $\langle a_f^2\rangle$ for fairly typical values of $D/l$ and $Re_\lambda$. For example, in the experiments of Mériaux *et al.*[8] ($D/l = 0.2$ and $Re_\lambda \approx 292 - 418$), the ratio of the acceleration variance from the particles to that from the flow is $\langle a_p^2\rangle/\langle a_f^2\rangle \approx 0.15$ (corresponding to a ratio of the RMS accelerations $\langle a_p^2\rangle^{1/2}/\langle a_f^2\rangle^{1/2} \approx 0.4$), which is a much larger underestimation than for the velocity variance.

## V. CONCLUSIONS

A model has been developed in this paper to evaluate the filtering effect of finite-sized neutrally-buoyant particles suspended in turbulence on statistical properties of the flow, namely the velocity and acceleration variances and the TKE dissipation rate, as obtained from the motion of the particles. The model uses the computationally inexpensive approach of representing this effect as a spatial filtering of the turbulent motion, where contributions to the turbulence spectrum coming from scales smaller than the size of the particles are suppressed, whereas those larger are retained. This entails adopting analytical energy spectra of the turbulence in both the wavenumber and frequency domains, which are related through a closure assumption. Hence, it is possible to calculate statistics both of the turbulent motion and of the motion of the particles, which are benchmarked against experimental and DNS data from 10 studies, for a range of Reynolds numbers. Through this procedure, the proposed model is validated before it is used to evaluate the particle filtering effect. The turbulence is assumed to be homogeneous and isotropic. The adopted wavenumber energy spectrum $E(k)$ is the Corrsin-Pao spectrum, possessing an inertial subrange and a smooth viscous cutoff. The adopted Lagrangian frequency spectrum $\phi(\omega)$ is a Lorenz spectrum, approaching a constant at low frequencies, and having an inertial subrange that decays as the inverse of the square of the frequency. For lack of a better widely-accepted choice, and also for mathematical simplicity, its viscous cutoff is assumed to be abrupt.

The model shows a variation of the dimensionless dissipation rate $\varepsilon'$ with the Taylor microscale Reynolds number $Re_\lambda$ that is in good agreement with a number of datasets, most of them for isotropic turbulence. The variations of the coefficient to which $\phi(\omega)$ is proportional $\beta$ (sometimes called the Kolmogorov constant, not to be confused with the Kolmogorov constant $\alpha$) and of the acceleration variance $\langle a_f^2 \rangle$ with $Re_\lambda$ also show good agreement with the most recent and comprehensive datasets. In particular, $\beta$ approaches a constant $\approx 2.31$ and $\langle a_f^2 \rangle \sim \varepsilon^{4/3}\eta^{-2/3}$ when $Re_\lambda \to \infty$, the latter being a well-known statistical property of turbulent flows. The values of $a_0 = \langle a_f^2 \rangle / (\varepsilon^{4/3}\eta^{-2/3})$ from some of the datasets used in the calibration and testing of the present model depart somewhat from the robust trend with $Re_\lambda$ found by Lawson *et al.*[26] and reproduced by the model in Fig. 4. In those cases, a correction to $a_0$ consistent with the turbulence model was found to substantially improve the agreement of the data with the particle motion statistics.

The model requires defining a number of adjustable coefficients, all of which appear in physically consistent definitions and take plausible values (being of $O(1)$ when they are constants of proportionality in definitions based on dimensional analysis). Their best fitted values were determined to be: $\alpha = 2$, $C_\infty = 0.58$, $\gamma = 5$, $a_1 = 0.8$, $a_2 = 2.5$, $b_1 = 0.84$, $b_2 = 3.3$ and (in the frequency energy spectrum) $k_D D = 3$. These coefficients define the calibration of the model used for quantifying the filtering of the turbulence statistics by the particles. This calibration is carried out via a number of comparisons of the filtered acceleration variance $\langle a_p^2 \rangle$ and velocity variance $q_p^2$ of the particles with laboratory and DNS data. In these comparisons, a relationship between the frequency and the wavenumber, approximately valid in the inertial subrange, allows expressing the spatial filtering inherent to the particles in the frequency domain. This relationship, in conjunction with the model for $\langle a_p^2 \rangle$ based on the frequency spectrum $\phi(\omega)$, enables deriving a scaling of the filtered acceleration variance as $Re_\lambda \to \infty$, $\langle a_p^2 \rangle \sim \varepsilon^{4/3} D^{-2/3}$, which is supported by previous studies. The relation between the frequency and the wavenumber ensures that $q_p^2$, either calculated from the wavenumber spectrum $E(k)$ or the frequency spectrum $\phi(\omega)$, are compatible. This constraint is not enforced exactly in the present model, but it is satisfied to a very good approximation for $D/l \leq 0.2$ and sufficiently high values of $Re_\lambda$ (as shown in Fig. 9). That is because, at high $Re_\lambda$, a well-developed inertial subrange exists in the turbulence spectrum, and hence the particles have a size that falls into this inertial subrange, where the relation between the frequency and the wavenumber, mentioned above, applies. These conditions are satisfied particularly well in laboratory experiments, where $Re_\lambda$ is often large, say $Re_\lambda \approx 500 - 1000$. The model fails when the size of the particles approaches a scale corresponding to the peak of the wavenumber spectrum $E(k)$ (i.e. approximately the integral length scale of the turbulence) or the Kolmogorov microscale $\eta$. In the latter case, the particles reach the dissipation range in the spectrum, so there is essentially no attenuation of the turbulence statistics. The fact that the adjusted constants $a_1$ and $b_1$, defining the high-frequency cutoffs of the energy spectrum of the fluid and particles, differ considerably from $a_2$ and $b_2$, defining the corresponding acceleration spectrum cutoffs, suggests that both the viscous tail of the frequency spectrum and the tail produced by truncation of the spectrum by particle filtering are not very steep, probably having an algebraic, rather than an exponential decay.

The model shows that, for a given particle diameter $D$ and Reynolds number $Re_\lambda$, the velocity variance probed by the particles $q_p^2$ underestimates much less the fluid velocity variance in the turbulence $q^2$ than the probed acceleration variance $\langle a_p^2 \rangle$ underestimates the true acceleration variance $\langle a_f^2 \rangle$, and even less than the probed dissipation rate $\varepsilon_p$ underestimates the true dissipation $\varepsilon$ (if these quantities are evaluated based on their primary definitions). This is because $\langle a_p^2 \rangle$ and $\varepsilon_p$ receive larger contributions from high wavenumbers/frequencies in the spectrum (which are those truncated by the particle motion) than $q_p^2$ does. When keeping $D/l$ fixed, $q_p^2/q^2$, $\varepsilon_p/\varepsilon$ and $\langle a_p^2 \rangle / \langle a_f^2 \rangle$ all decrease as $Re_\lambda$ increases, because the fraction of the energy spectrum existing above the cutoff wavenumber/frequency imposed by the parti-

cles becomes progressively larger. In particular, it can be shown that for sufficiently high $Re_\lambda$, $\varepsilon_p/\varepsilon \propto Re_\lambda^{-2}$ and $\langle a_p^2\rangle/\langle a_f^2\rangle \propto Re_\lambda^{-1}$. It was found that, for the conditions considered in Mériaux *et al.*[8] ($D/l = 0.2$ and $Re_\lambda = 292 - 418$), $q_p^2/q^2 \approx 0.8$ (or $q_p/q \approx 0.9$) and $\langle a_p^2\rangle/\langle a_f^2\rangle \approx 0.15$ (or $\langle a_p^2\rangle^{1/2}/\langle a_f^2\rangle^{1/2} \approx 0.4$). In other words, although quite large particles severely underestimate the acceleration magnitude in the turbulence, they typically underestimate the RMS velocity only slightly.

These effects have been illustrated by previous authors for specific cases, but the present study provides a framework to evaluate them systematically, helping to specify the conditions under which finite-sized particles may be considered equivalent to tracers for the purpose of estimating different turbulence statistics. The concept of using finite-sized particles for probing some carefully-chosen turbulence properties contrasts with usual practice and opens up new possibilities. Since it is possible to derive spatial structure functions using pairs of finite-sized particles[8], as long as the particles fall within the inertial subrange of turbulence, the error affecting these statistics is comparable to that affecting the velocity variance. Therefore, in the context of laboratory experiments, the energy dissipation rate could be estimated without too much error via the velocity structure functions without resorting to tracers (which require a specific laboratory setup of particle image velocimetry (PIV) based on laser), but using instead a few finite-sized neutrally buoyant particles tracked by a simple camera. Additionally, the fact that the turbulent flow model underlying the particle filtering model predicts with good accuracy various statistics of the turbulent flow itself for an even wider range of Reynolds numbers suggests that it might also be useful for more general purposes.

## ACKNOWLEDGMENTS

C. A. Mériaux warmly thanks Profs. Peter Betts and Andrew Mackintosh from the School of Earth, Atmosphere and Environment of Monash University for their support.

[1]Y. Sato and K. Yamamoto, "Lagrangian measurement of fluid-particle motion in an isotropic turbulent field," J. Fluid Mech. **175**, 183–199 (1987).
[2]N. Mordant, P. Melz, O. Michel, and J.-F. Pinton, "Measurement of lagrangian velocity in fully-developed turbulence," Phys. Rev. Lett. **21**, 214501 (2001).
[3]N. T. Ouellette, H. Xu, M. Bourgoin, and E. Bodenschatz, "An experimental study of turbulent relative dispersion models," New. J. Phys. **8**, 109 (2006).
[4]P. J. Ireland, A. D. Bragg, and L. R. Collins, "The effect of reynolds number on inertial particle dynamics in isotropic turbulence. part 1. simulations without gravitational effects," J. Fluid Mech. **796**, 617–658 (2016).
[5]M. Uhlmann and A. Chouippe, "Clustering and preferential concentration of finite-size particles in forced homogeneous-isotropic turbulence," J. Fluid Mech. **812**, 991–1023 (2017).
[6]N. M. Qureshi, M. Bourgoin, C. Baudet, A. Cartellier, and Y. Gagne, "Turbulent transport of material particles: an experimental study of finite size effects," Phys. Rev. Lett. **99**, 184502 (2007).
[7]R. Volk, E. Calzavarini, E. Lévêque, and J.-F. Pinton, "Dynamics of inertial particles in a turbulent von kármán flow," J. Fluid Mech. **668**, 223–235 (2011).
[8]C. A. Mériaux, M. A. C. Teixeira, J. J. Monaghan, R. Cohen, and P. Cleary, "Dispersion of finite-size particles probing inhomogeneous and anisotropic turbulence," Eur. J. Mech. B - Fluids **84**, 93–109 (2020).
[9]J. Bec, L. Biferale, G. Boffetta, A. Celani, M. Cencini, A. Lanotte, S. Musacchio, and F. Toschi, "Acceleration statistics of heavy particles in turbulence," J. Fluid Mech. **550**, 349–358 (2006).
[10]J. P. L. C. Salazar and L. R. Collins, "Inertial particle acceleration statistics in turbulence: effects of filtering, biased sampling, and flow topology," Phys. Fluids **24**, 083302 (2012).
[11]N. Machicoane and R. Volk, "Lagrangian velocity and acceleration correlations of large inertial particles in a closed turbulent flow," Phys. Fluids **28**, 035113 (2016).
[12]E. Calzavarini, R. Volk, E. Lévêque, J.-F. Pinton, and F. Toschi, "Impact of trailing wake drag on the statistical properties and dynamics of finite-sized particle in turbulence," Physica D **241**, 237–244 (2012).
[13]R.-C. Lien, E. A. D'Asaro, and G. T. Dairiki, "Lagrangian frequency spectra of vertical velocity and vorticity in high-reynolds-number oceanic turbulence," J. Fluid Mech. **362**, 177–198 (1998).
[14]R.-C. Lien and E. A. D'Asaro, "Measurement of turbulent kinetic energy dissipation rate with a lagrangian float," J. Atmos. Ocean. Thechnol. **23**, 964–976 (2006).
[15]C. C. Lalescu and M. Wilczek, "Acceleration statistics of tracer particles in filtered turbulent fields," J. Fluid Mech. **847**, R2 (2018).
[16]E. Calzavarini, R. Volk, M. Bourgoin, E. Lévêque, J.-F. Pinton, and F. Toschi, "Acceleration statistics of finite-sized particles in turbulent flow: the role of faxén forces," J. Fluid Mech. **630**, 179–189 (2009).
[17]R. D. Brown, Z. Warhaft, and G. A. Voth, "Acceleration statistics of neutrally buoyant spherical particles in intense turbulence," Phys. Rev. Lett. **103**, 194501 (2009).
[18]P. K. Yeung, "Lagrangian characteristics of turbulence and scalar transport in direct numerical simulations," J. Fluid Mech. **427**, 241–274 (2001).
[19]H. Homann and J. Bec, "Finite-size effects in the dynamics of neutrally buoyant particles in turbulent flow," J. Fluid Mech. **651**, 81–91 (2010).
[20]J. J. Monaghan and C. A. Mériaux, "What can we learn from large bodies moving in a turbulent fluid," Eur. J. Mech. B. - Fluids **72**, 519–530 (2018).
[21]B. L. Sawford, "Reynolds number effects in lagrangian stochastic models of turbulent dispersion," Phys. Fluids A **3**, 1577–1586 (1991).
[22]F. Lucci, V. S. L'vov, A. Ferrante, M. Rosso, and S. Elgobashi, "Eulerian-lagrangian bridge for the energy and dissipation spectra in isotropic turbulence," Theor. Comput. Fluid Dyn. **28**, 197–213 (2014).
[23]G. A. Voth, K. Satyanarayan, and E. Bodenschatz, "Lagrangian acceleration measurements at large reynolds number," Phys. Fluids **10**, 2268–2280 (1998).
[24]R. J. Hill, "Scaling of acceleration in locally isotropic turbulence," J. Fluid Mech. **452**, 361–370 (2002).
[25]B. L. Sawford, P. K. Yeung, M. S. Borgas, P. Vedula, A. L. Porta, A. M. Crawford, and E. Bodenschatz, "Conditional and unconditional acceleration statistics in turbulence," Phys. Fluids **15**, 3478–3489 (2003).
[26]J. M. Lawson, E. Bodenschatz, C. C. Lalescu, and M. Wilczek, "Bias in particle tracking acceleration measurement," Exper. Fluids **59**, 172 (2018).
[27]B. L. Sawford, P. K. Yeung, and J. F. Hackl, "Reynolds number dependence of relative dispersion statistics in isotropic turbulence," Phys. Fluids **20**, 065111 (2008).

[28]R.-C. Lien and E. A. D'Asaro, "The kolmogorov constant for the lagrangian velocity spectrum and structure function," Phys. Fluids **14**, 4456–4459 (2002).
[29]P. K. Yeung, S. B. Pope, A. G. Lamorgese, and D. A. Donzis, "Acceleration and dissipation statistics of numerically simulated isotropic turbulence," Phys. Fluids **18**, 065103 (2006).
[30]M. Barjona and C. B. da Silva, "Kolmogorov's lagrangian similarity law revisited," Phys. Fluids **29**, 105106 (2017).
[31]F. Toschi and E. Bodenschatz, "Lagrangian properties of particles in turbulence," Ann. Rev. Fluid Mech. **41**, 375–404 (2009).
[32]M. A. C. Teixeira and S. E. Belcher, "Dissipation of shear-free turbulence near boundaries," J. Fluid Mech. **422**, 167–191 (2000).
[33]H. Tennekes and J. L. Lumley, A First Course in Turbulence (MIT Press, 1972) p. 300 pp.
[34]S. B. Pope, Turbulent Flows (Cambridge University Press, 2000) p. 771 pp.
[35]J. C. R. Hunt and J. M. R. Graham, "Free stream turbulence near plane boundaries," J. Fluid Mech. **84**, 209–235 (1978).
[36]T. Ishihara, T. Gotoh, and Y. Kaneda, "Study of high-reynolds number isotropic turbulence by direct numerical simulation," Ann. Rev. Fluid Mech. **41**, 165–180 (2009).
[37]W. D. McComb, A. Berera, S. R. Yoffe, and M. F. Linkmann, "Energy transfer and dissipation in forced isotropic turbulence," Phys. Rev. E **91**, 043013 (2015).
[38]L. Djendi, N. Lefeuvre, M. Kamruzzaman, and R. A. Antonia, "On the normalized dissipation parameter $c_\epsilon$ is decaying turbulence," J. Fluid Mech. **817**, 61–79 (2017).
[39]A. S. Monin and A. M. Yaglom, Statistical Fluid Mechanics: Mechanics of Turbulence, volume 2 (MIT Press, 1981) p. 874 pp.
[40]Y. Huang, L. Biferale, E. Calzavarini, C. Sun, and F. Toschi, "Lagrangian single-particle turbulent statistics through the hilbert-huang transform," Phys. Rev. E **87**, 041003(R) (2013).
[41]P. K. Yeung, S. B. Pope, and B. L. Sawford, "Reynolds number dependence of lagrangian statistics in large numerical simulations of isotropic turbulence," J. Turbul. **7**, N58 (2006).
[42]R. Mei and R. J. Adrian, "Effect of reynolds number on isotropic turbulent dispersion," Trans. ASME **117**, 402–409 (1995).
[43]P. K. Yeung, "Lagrangian investigations of turbulence," Ann. Rev. Fluid Mech. **34**, 115–142 (2002).
[44]G. A. Voth, A. L. Porta, A. M. Crawford, J. Alexander, and E. Bodenschatz, "Measurement of particle accelerations in fully developed turbulence," J. Fluid Mech. **469**, 121–160 (2002).
[45]K. Yeo, S. Dong, E. Climent, and M. R. Maxey, "Modulation of homogeneous turbulence seeded with finite-size bubbles or particles," Int. J. Multiphase Flow **36**, 221–233 (2010).
[46]M. Gibert, H. Xu, and E. Bodenschatz, "Inertial effects on two-particle relative dispersion in turbulent flows," Europhys. Lett. **90**, 64005 (2010).
[47]A. Jabbari, A. Rouhi, and L. Boegman, "Evaluation of the structure function method to compute turbulent dissipation within boundary layers using numerical simulations," J. Geophys. Res. Oceans **121**, 5888–5897 (2016).
[48]N. Penna, E. Padhi, S. Dey, and R. Gaudio, "Structure functions and invariants of the anisotropic reynolds stress tensor in turbulent flows over water-worked gravel beds," Phys. Fluids **32**, 055106 (2020).

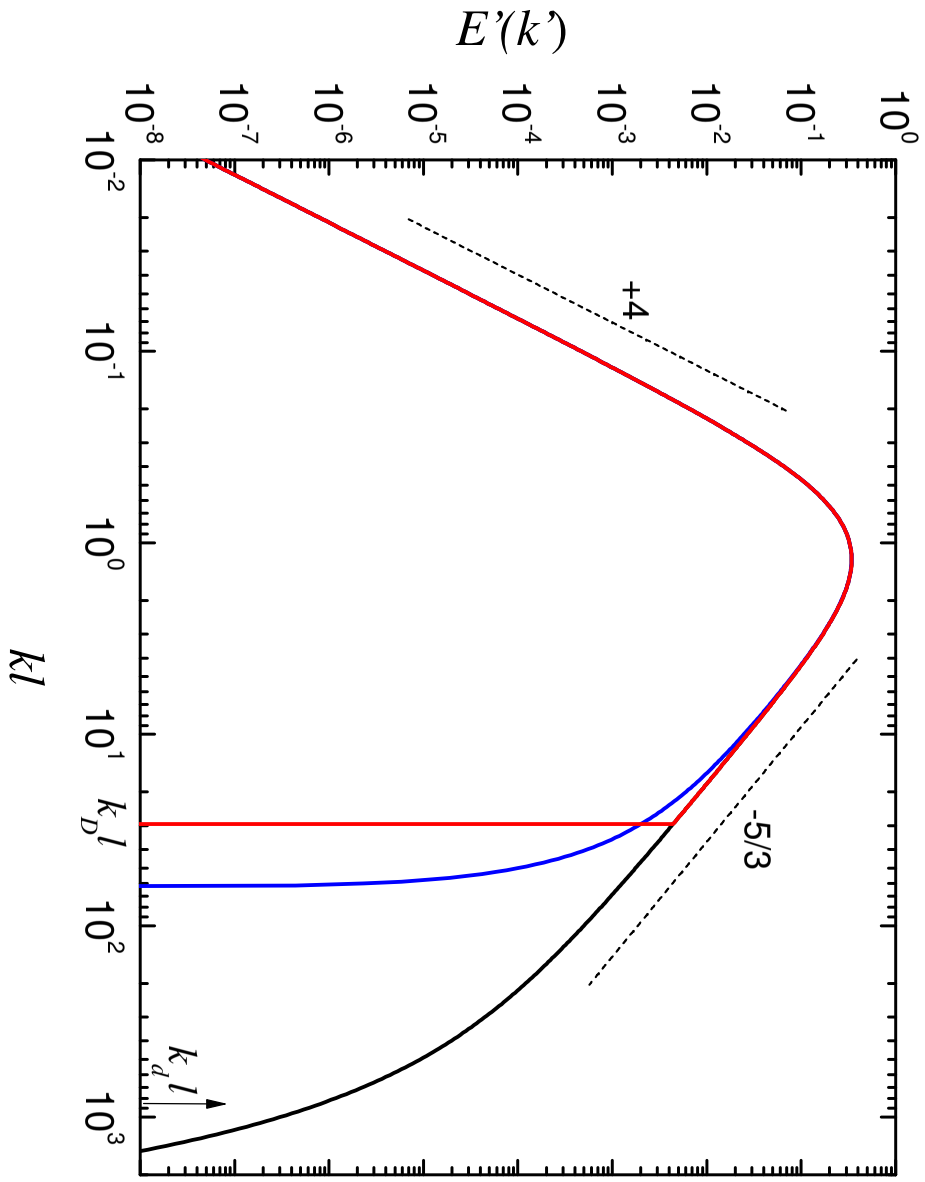

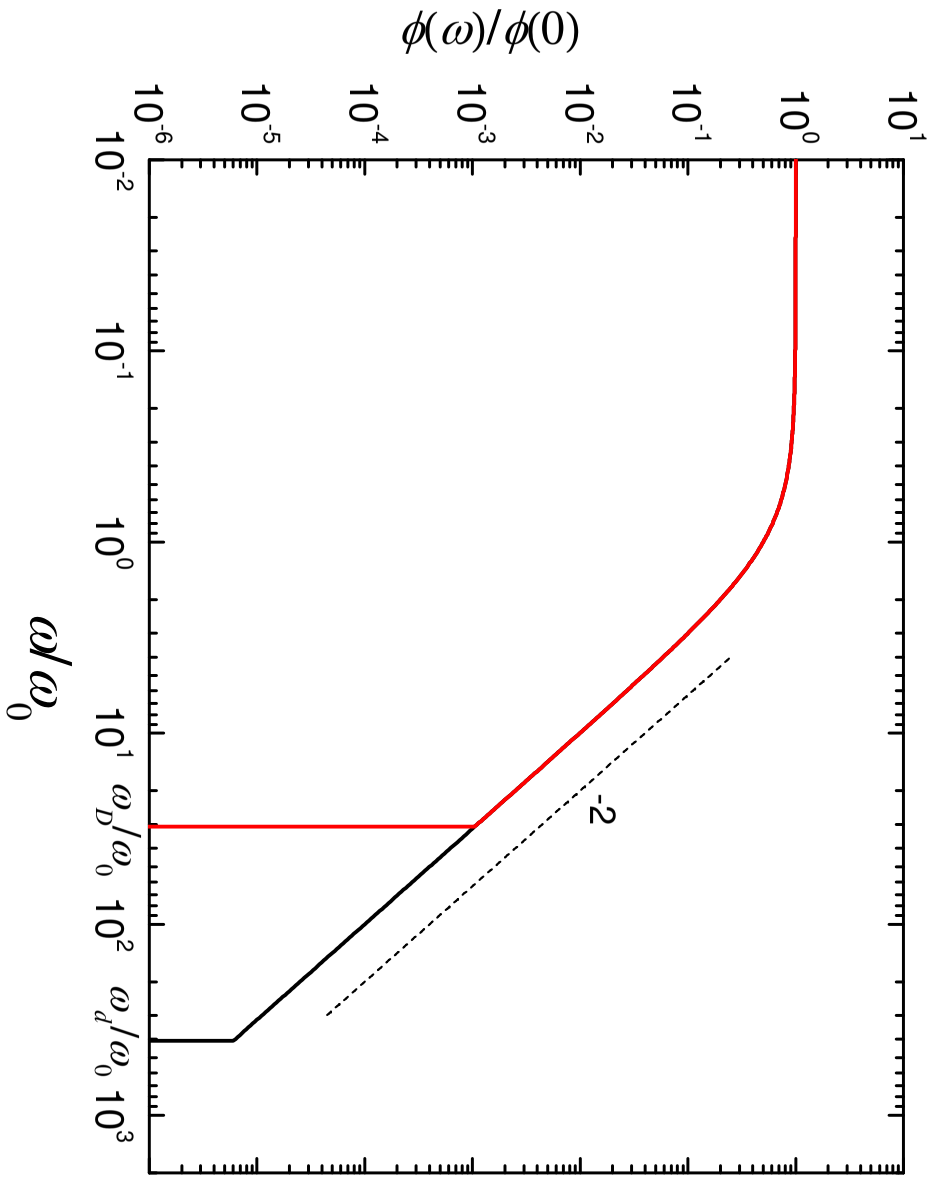

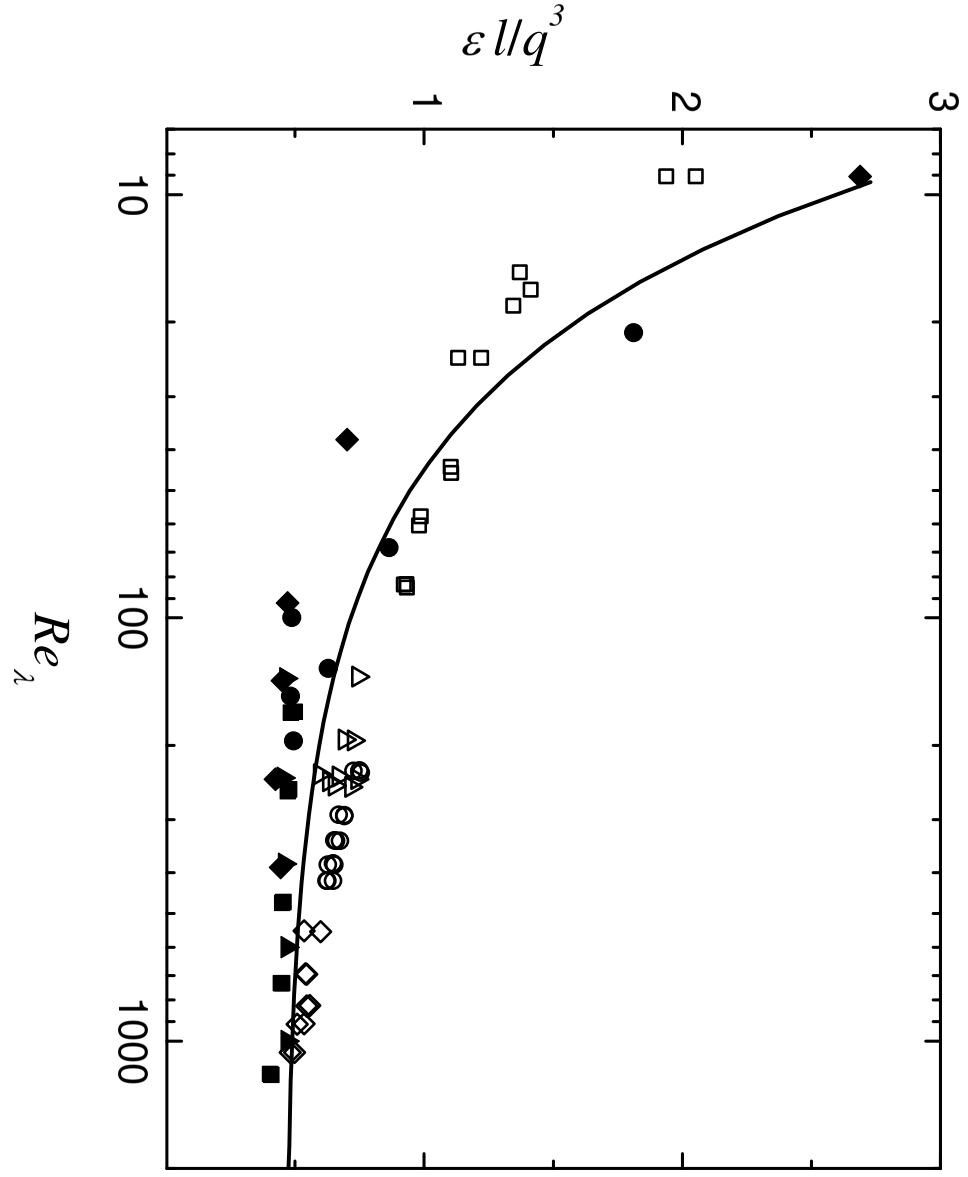

PLEASE CITE THIS ARTICLE AS DOI: 10.1063/5.0084622

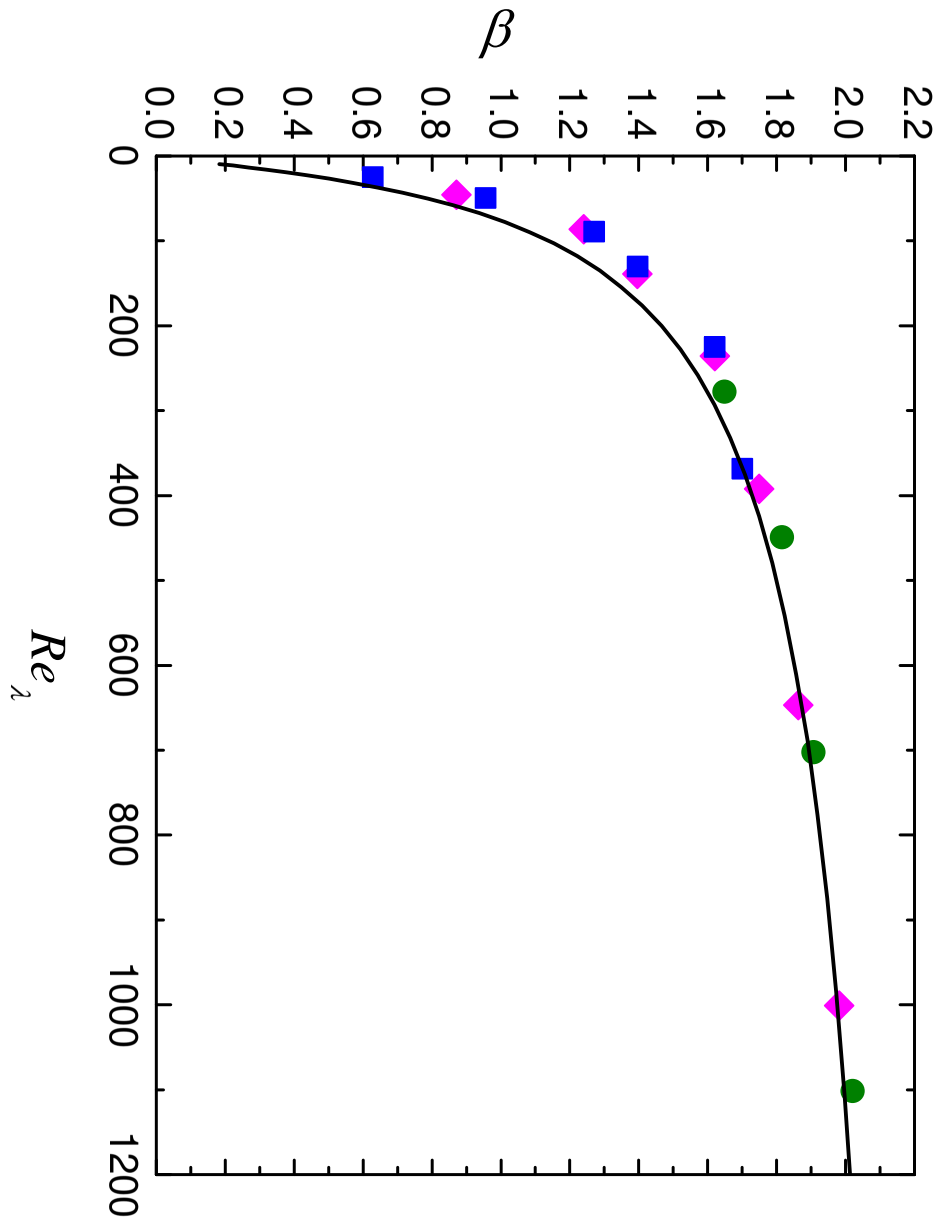

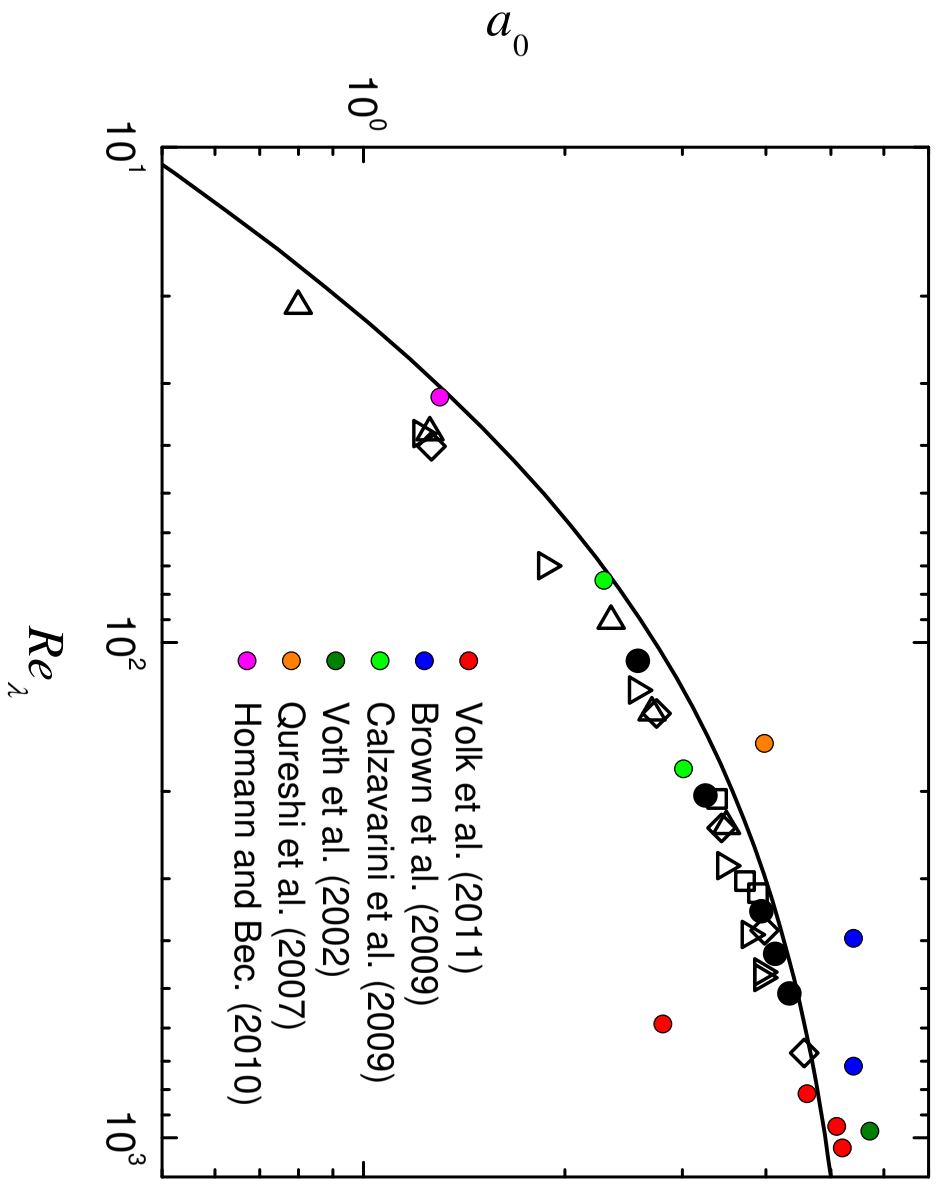

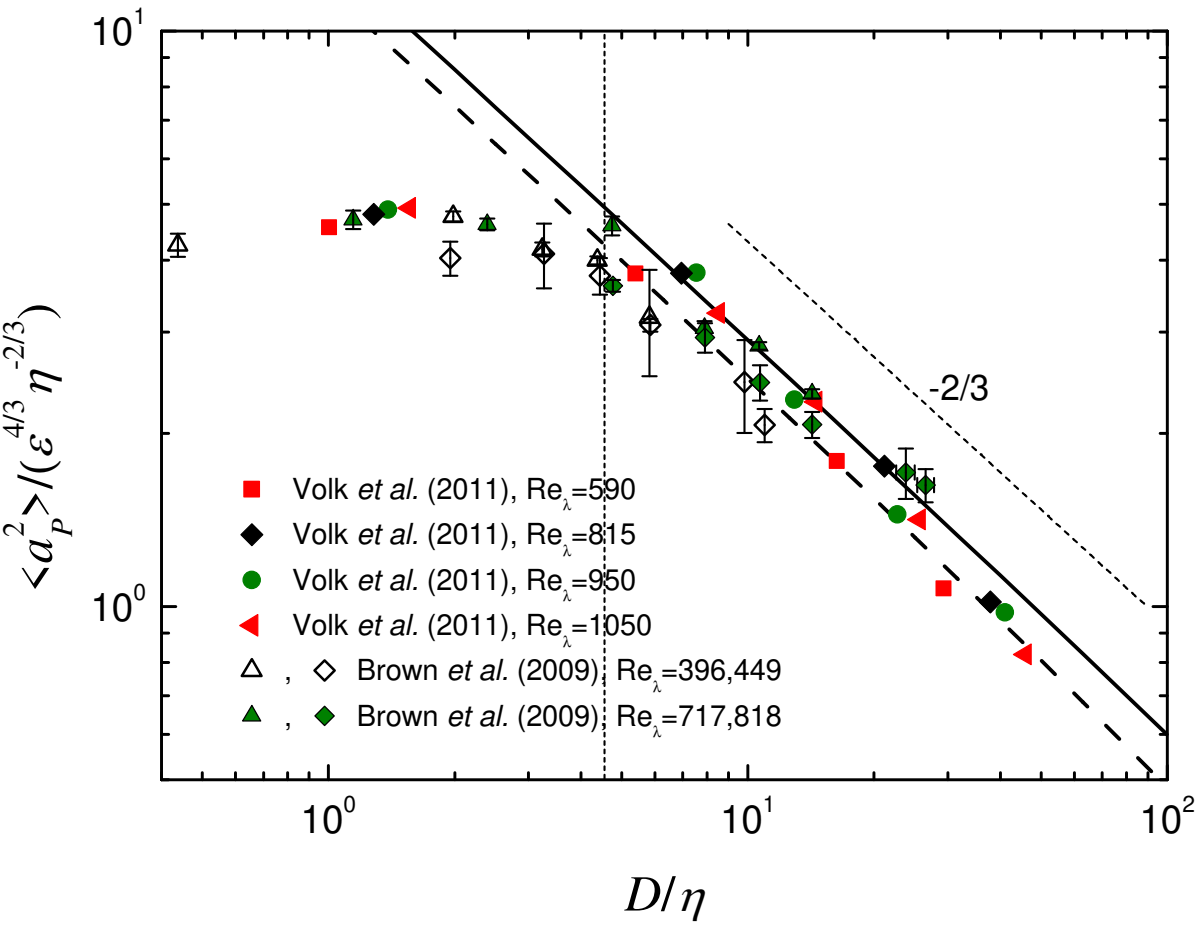

PLEASE CITE THIS ARTICLE AS DOI: 10.1063/5.0084622

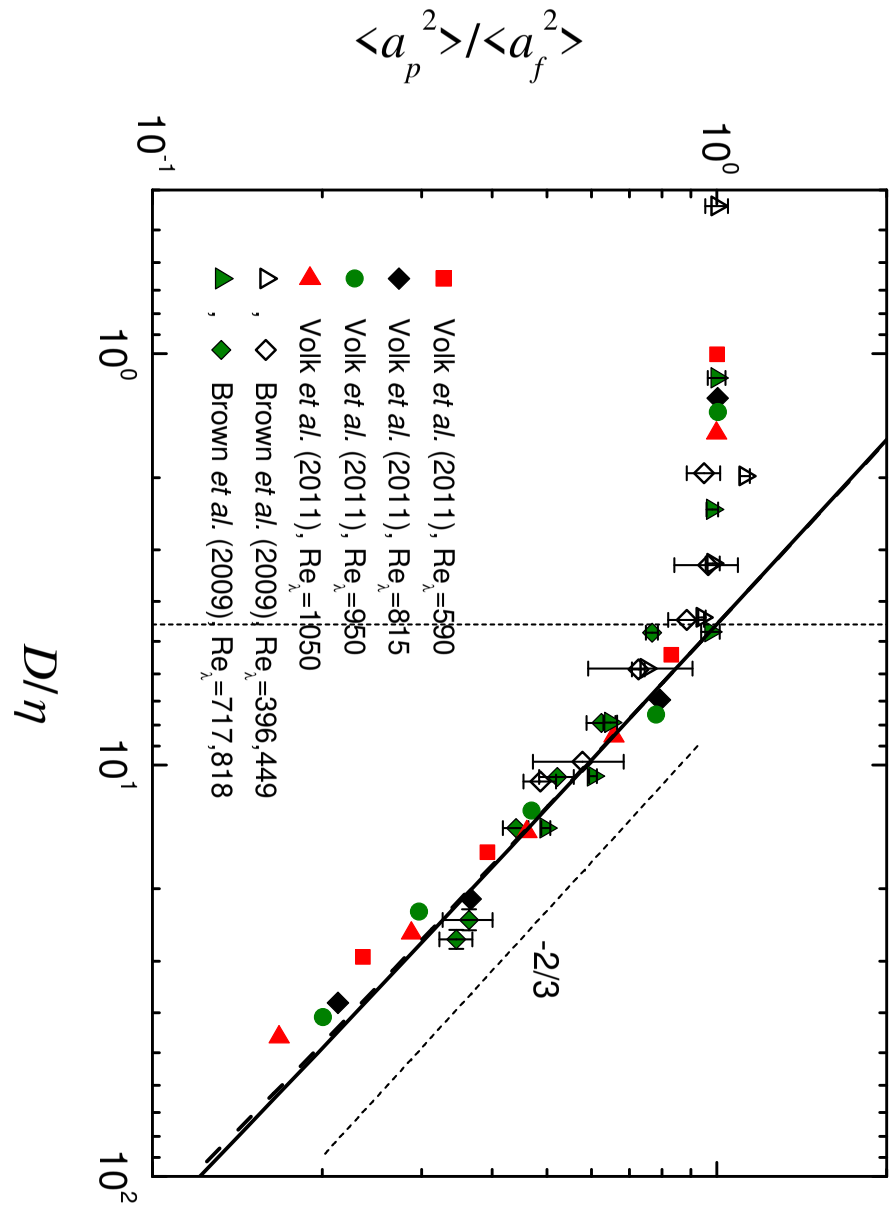

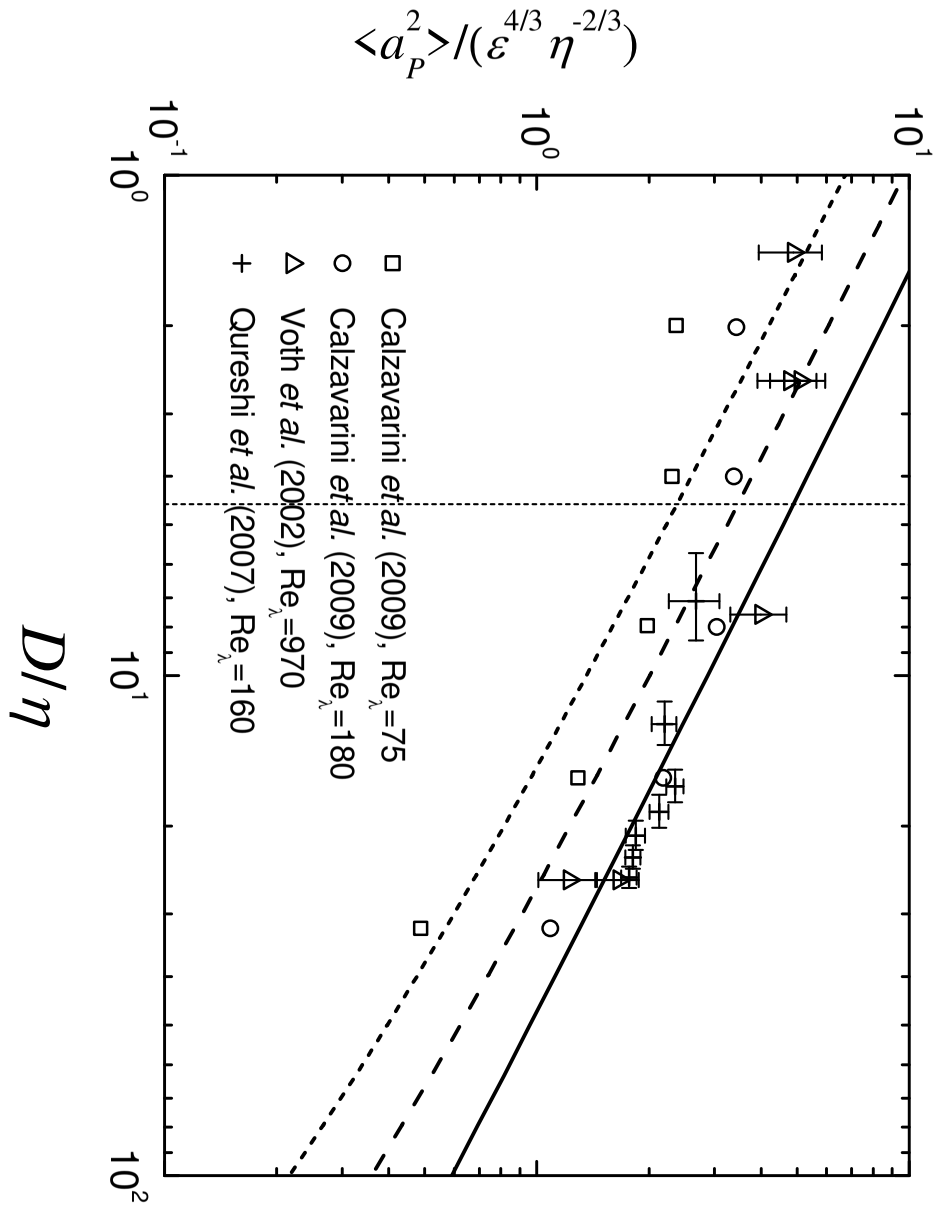

PLEASE CITE THIS ARTICLE AS DOI: 10.1063/5.0084622

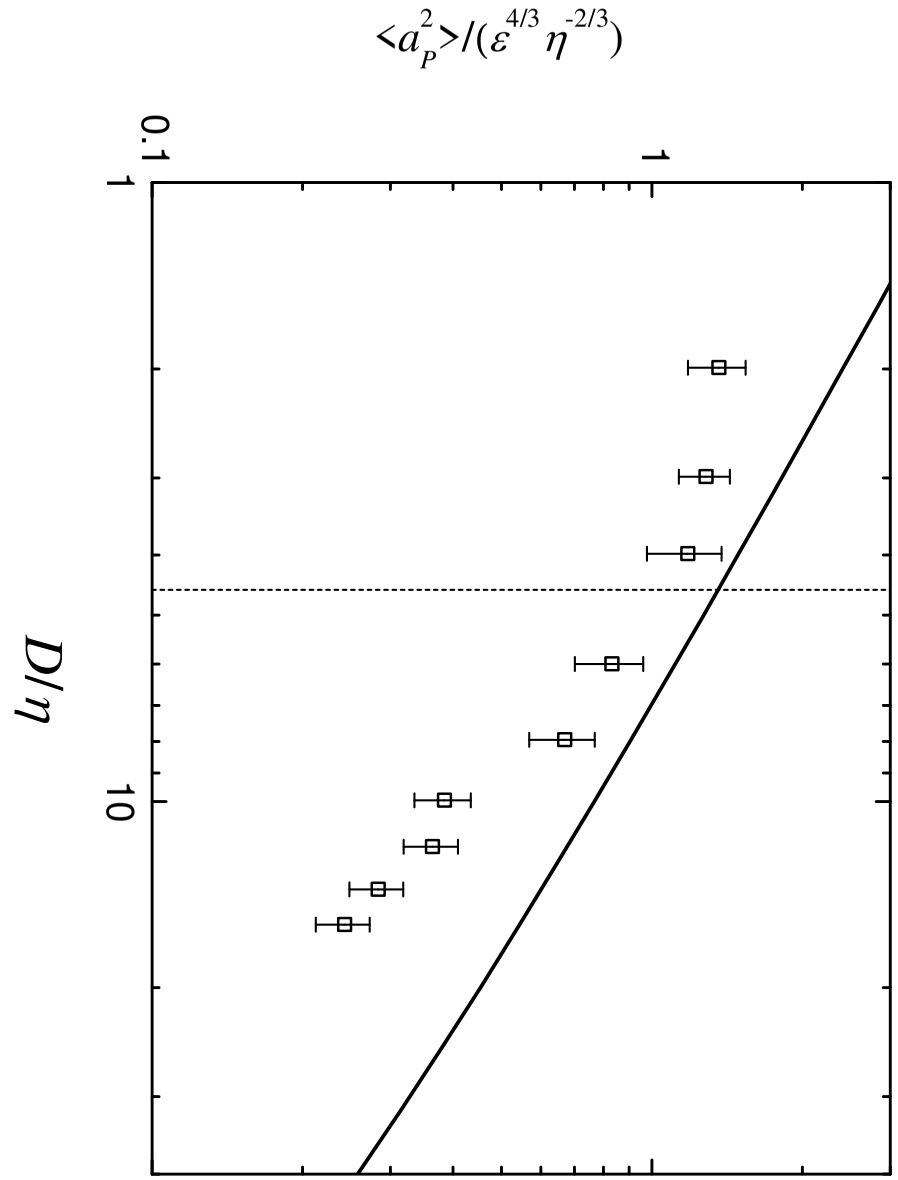

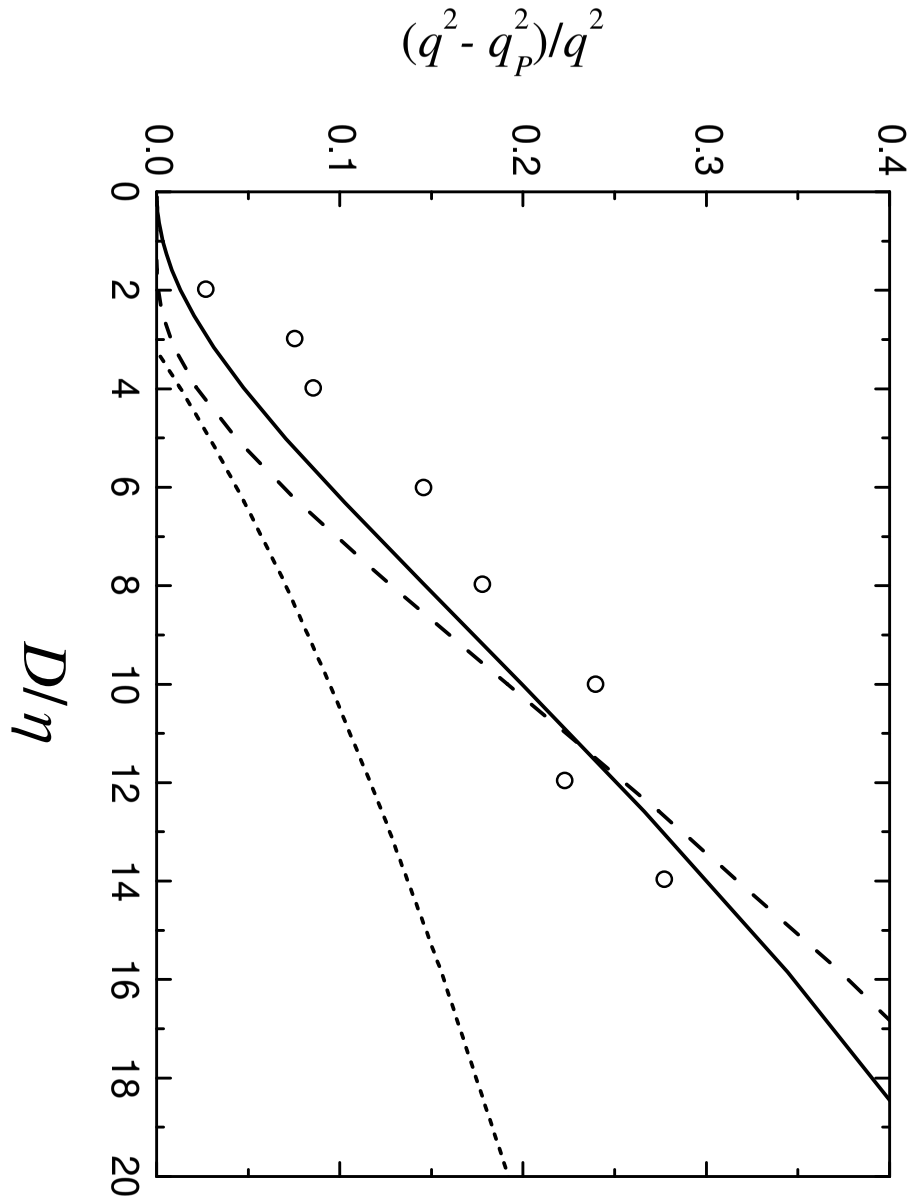

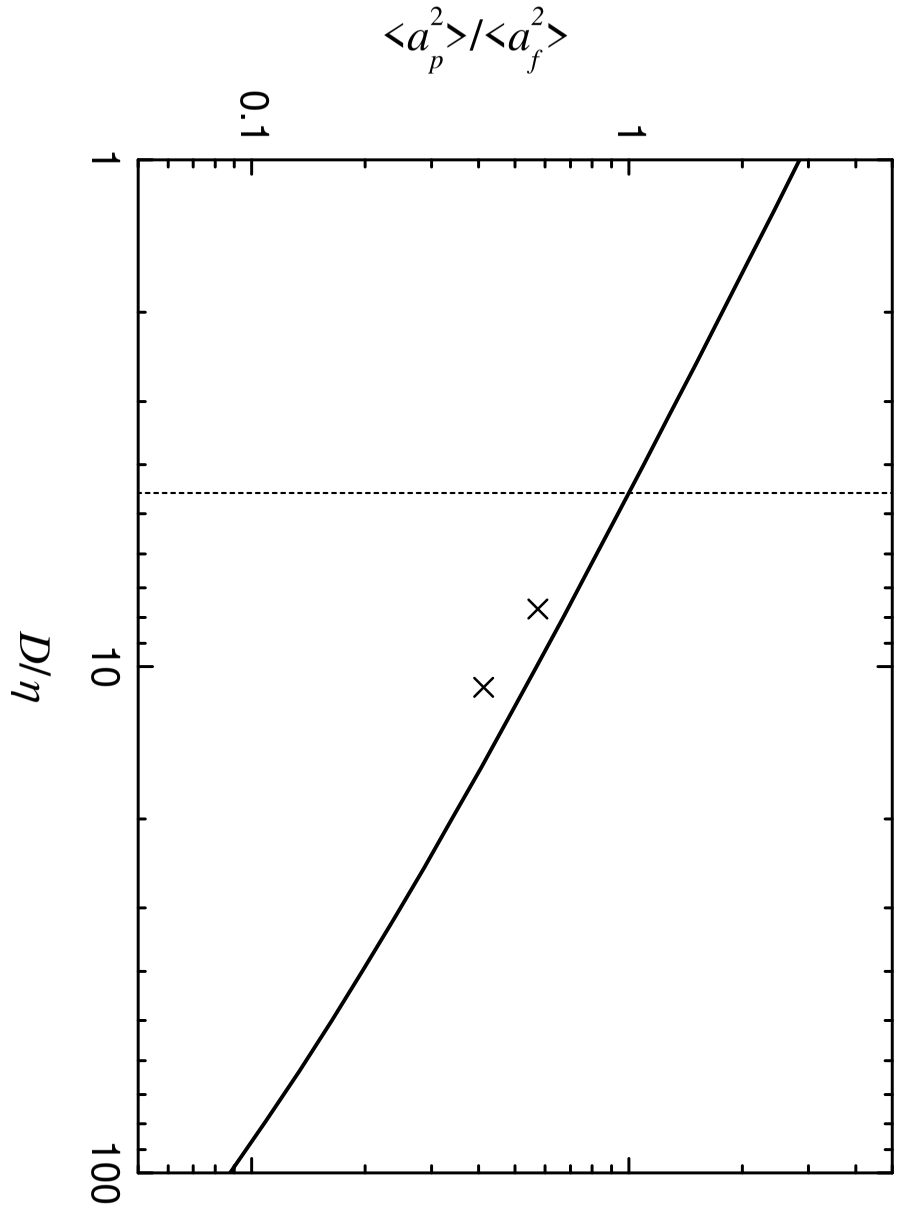

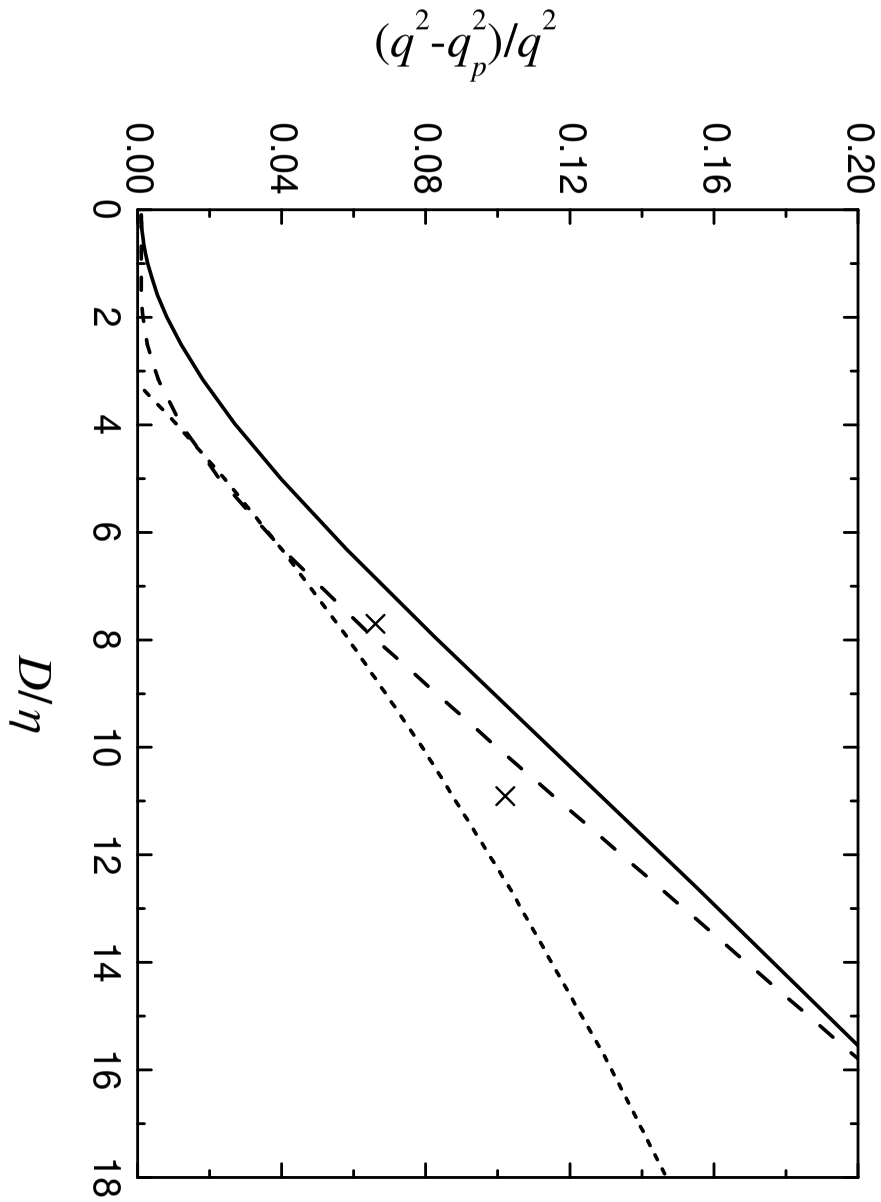

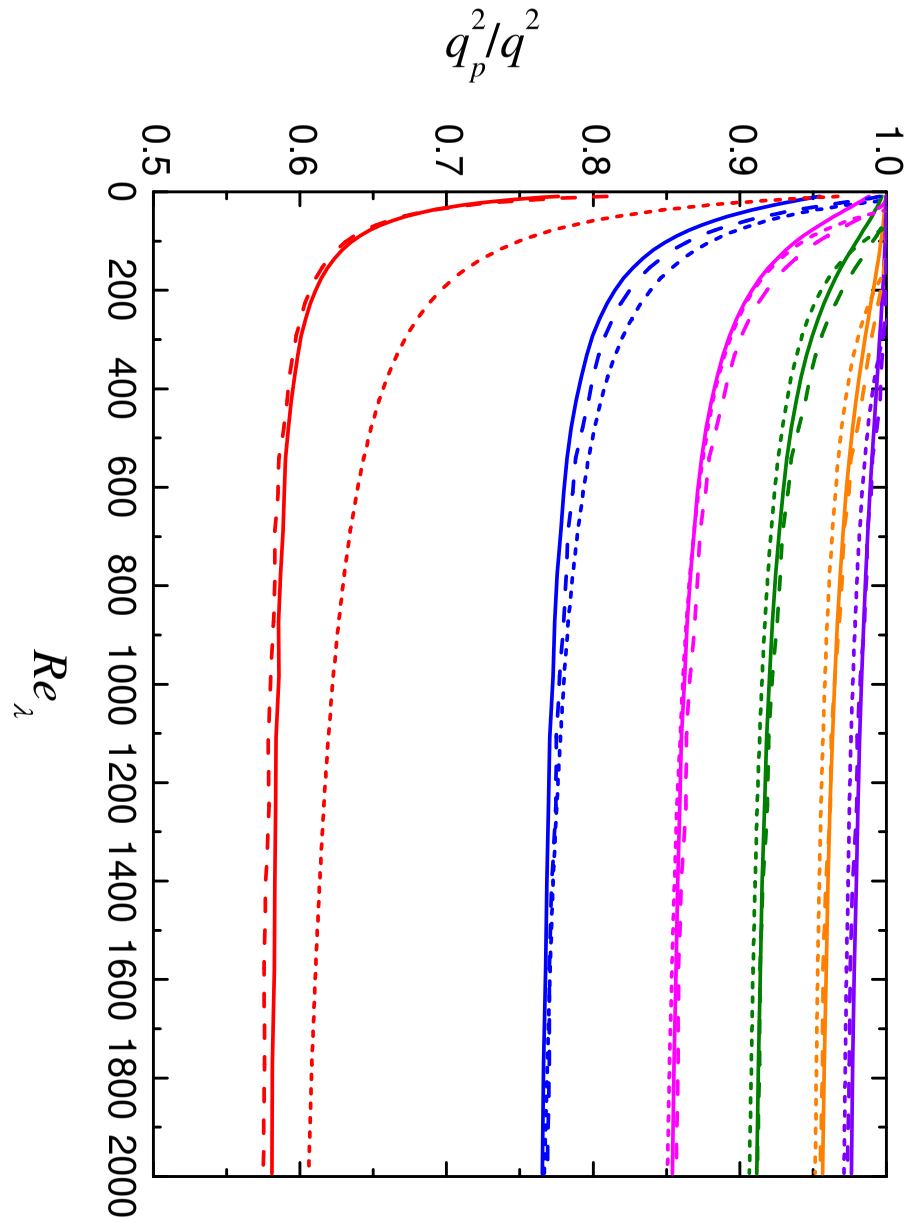

PLEASE CITE THIS ARTICLE AS DOI: 10.1063/5.0084622

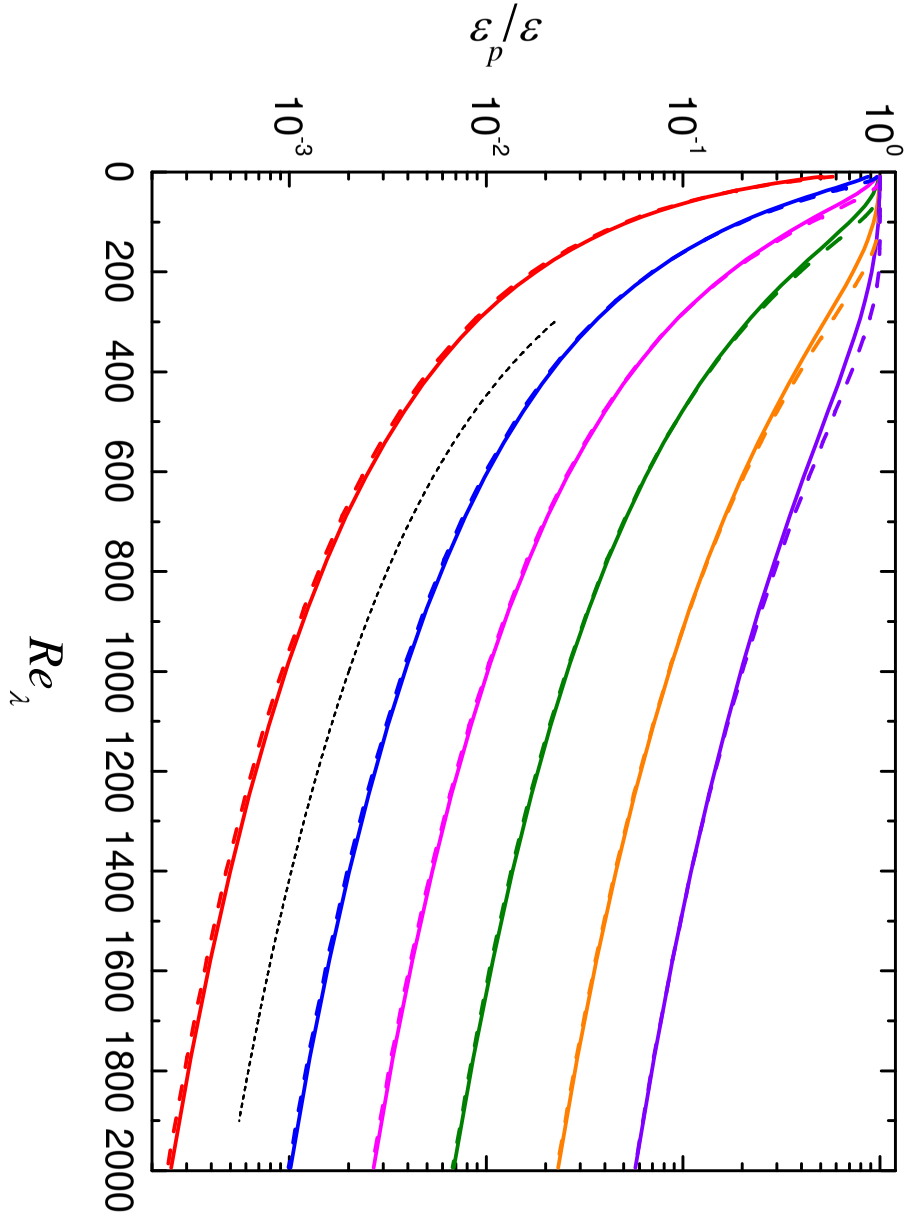

PLEASE CITE THIS ARTICLE AS DOI: 10.1063/5.0084622